Laser Sources For Generation of Ultrasound

Contract No. NAG-1-1524

Final Technical Report

Prepared for the
National Aeronautics and Space Administration
Langley Research Center
Hampton, VA 23665

James W. Wagner
Johns Hopkins University
Department of Materials Science & Engineering
Baltimore, MD 21218

Laser Sources for Generation of Ultrasound

James W. Wagner
Department of Materials Science and Engineering
Johns Hopkins University
Baltimore, MD 21218

Abstract

Two laser systems have been built and used to demonstrate enhancements beyond current technology used for laser-based generation and detection of ultrasound. The first system consisted of ten Nd:YAG laser cavities coupled electronically and optically to permit sequential bursts of up to ten laser pulses directed either at a single point or configured into a phased array of sources. Significant enhancements in overall signal-to-noise ratio for laser ultrasound incorporating this new source system was demonstrated, using it first as a source of narrowband ultrasound and secondly as a phased array source producing large enhanced signal displacements.

A second laser system was implemented using ultra fast optical pulses from a Ti:Sapphire laser to study a new method for making laser generated ultrasonic measurements of thin films with thicknesses on the order of hundreds of angstroms. Work by prior investigators showed that such measurements could be made based upon fluctuations in the reflectivity of thin films when they are stressed by an arriving elastic pulse. Research performed using equipment purchased under this program showed that a pulsed interferometric system could be used as well as a piezoreflective detection system to measure pulse arrivals even in thin films with very low piezoreflective coefficients.

LASER SOURCES FOR GENERATION OF ULTRASOUND

Objective: Establish capabilities for generation of narrowband, phased array, and picosecond ultrasonic signals using laser sources.

Background

Laser ultrasonics technology has been demonstrated to provide several advantages over conventional ultrasonic transduction methods owing to the ability to perform ultrasonic inspection tasks in a noncontact and remote fashion. The use of laser ultrasonic technology has found broad application in laboratory environments and, in an increasing number of cases, is expanding to the realm of industrial and field application. The goal of the efforts undertaken in this program was to broaden the applicability of laser ultrasonic methods by two means. In both cases the focus of the improvements was upon appropriate modification and design of laser systems used to generate ultrasonic signals in bulk materials and in thin films or coatings. In the first case, a new generation laser system was fully implemented to produce bursts of laser pulses when triggered instead of a single Q-switched laser spike normally produced by lasers used for ultrasonic pulse generation. Concurrently, laser system components were specified, purchased, and assembled to permit laser ultrasonic excitation of thin films and coatings using picosecond laser pulses. The results of studies from each of these systems have, in the first case, been submitted for publication in the journal *Ultrasonics*. The second aspect of the program was documented in a PhD dissertation. The remainder of this report is comprised of material excerpted from those two manuscripts.

I: Experimental Evaluation of Enhanced Generation of Ultrasonic Waves Using an Array of Laser Sources

From a manuscript submitted to *Ultrasonics* by
T. W. Murray and J. W. Wagner

Introduction

The principles and uses of optical techniques for generation and detection of ultrasound have been discussed extensively in the literature.[1] The major advantages of using laser ultrasonic techniques over the conventional piezoelectric transducer techniques for materials characterization and industrial inspection applications are that laser methods are non-contact (no surface couplants need be applied) and they are remote (may be used in hostile environments). The primary disadvantage of using these systems, though, is that acoustic signals generated by pulsed laser sources in the thermoelastic regime have relatively low amplitudes. Considering the low sensitivity of typical optical detection systems, these signals are generally quite difficult to detect. For truly nondestructive applications of laser ultrasonics, the generation of ultrasound must take place in the thermoelastic regime such that damage to the surface of the specimen of interest can be avoided. Consequently, the maximum power density which may be delivered to the specimen by a single laser source is limited by the ablation threshold of the material under inspection. This threshold is approximately 15 MW/cm^2 in aluminum,[2] for example.

Minimizing these limitations has been the goal of investigations to devise methods for increasing the sensitivity of laser ultrasonic systems. Improved system detection sensitivity can be achieved either by improving the sensitivity of the optical detection system or by increasing the efficiency of the laser generation system. Methods for increasing the sensitivity of optical detection systems, such as the use of high power detection lasers[3] and/or the use of the Fabry-Perot interferometer[4] for instance, have been discussed elsewhere and are outside of the scope of the present work. On the other hand, the efficiency of laser generation systems may be improved by surface modification[5] or by using an array of laser sources.[6] Surface modification can lead to a more efficient conversion from optical to acoustic energy resulting in larger amplitude displacements. If contact with the specimen is to be completely avoided, either due to the nature of the sample under interrogation or the experimental conditions, then surface modification may not be possible. The efficiency of laser generation may be improved by using an array of laser sources in two ways, each of which allows for the generation mechanism to remain in the thermoelastic, nondestructive regime. First, one may spatially and temporally modulate a series of laser pulses on the surface of a specimen, much like a phased array antenna, so that the acoustic waves generated by each laser source array element arrive at the detection point simultaneously. This concept is illustrated in *Figure 1* depicting a series of laser pulses impinging on a sample with pulse modulation parameters chosen such that wavefront superposition occurs at the detection point. In this manner the surface displacement at the detection point is increased allowing for greater detectability of the acoustic event. The second method of increasing the detection sensitivity of the system is shown in *Figure 2*. In this case, a series of laser pulses is spatially and/or temporally modulated on the surface of a specimen such that the acoustic waves generated by each of the laser pulses arrive at the detection point with a fixed temporal spacing, Δ t. A

narrow-band tone-burst of acoustic energy is observed at the detection point with the acoustic energy centered around the fundamental frequency ($1/\Delta$ t) and the corresponding harmonics. The bandwidth of the optical detection system can then be matched, through analog or digital filtering techniques, to that of the narrow-band acoustic signal. This reduction in the generated acoustic pulse train bandwidth, combined with a reduction in detection bandwidth, allows for the detection of the narrow-band signal energy and simultaneously provides for the rejection of much of the broad-band noise energy. The sensitivity of the system is thus increased through this noise reduction.

Arrays of laser sources have been produced by several different means. Prior investigators have reported using optical diffraction gratings,[7] lenticular arrays,[8] and interference patterns[9] to deliver laser energy simultaneously to a series of points or lines on a specimen and to generate narrow-band acoustic signals. Temporal arrays, also used for the generation of narrow-band ultrasound, have been produced by using a repetitively pulsed Q-switched Nd:YAG laser[10] and later using long cavity mode-locked Nd:YAG laser.[11] These laser sources deliver a series of pulses to a single point on a specimen. Systems capable of both spatial and temporal modulation and which allow for the generation of narrow-band or phased acoustic signals, have been produced using multiple fiber optic delays,[12] multiple laser cavities,[13] and a White cell optical delay cavity system.[14] The most flexible of these systems is the multiple laser cavity source. A relatively inexpensive implementation of a ten cavity laser array source was developed for these studies.

Theory

The signal-to-noise ratio, SNR_{power}, with which a shot noise limited optical detection system can detect small displacements, may be given as: [15]

$$SNR_{power} = \frac{signal\ power}{noise\ power} \propto \frac{\delta^2 P}{B} \qquad (1)$$

where δ is the amplitude of the surface displacement to be detected, P is the optical power from the detection laser incident on the detector, and B is the bandwidth of the detection system. By maximizing this quantity, the detection sensitivity of a laser-ultrasonic system can be optimized. As noted earlier, others have employed stable high power lasers for the detection of sound, thereby enhancing the SNR by increasing P. The focus of this work was to demonstrate SNR enhancement using laser array sources either to increase δ or to decrease B.

The use of a phased array provides one means to increase δ at some detection point. As is illustrated in *Figure* 1, a series of laser pulses impinge on the specimen at various points and are temporally modulated such that the resulting acoustic signals arrive at the detection point simultaneously. The total surface displacement at the detection point as a result of N generating sources may be given simply as:

$$\delta_{total} = \sum_{1}^{N} \frac{1}{R_n^m} D_N(\theta) A(t, \Delta t_N + \frac{r_N}{c}) I_N \qquad (2)$$

where R is a spherical propagation factor giving the geometrical loss resulting from beam spread, with m taking on a value consistent with geometrical spreading in two dimensions for the Rayleigh wave (.5) and three dimensions for the shear and longitudinal waves (1). D is the directivity function associated with the generating source and acoustic wave type (shear, longitudinal, or Rayleigh). A is an array factor (a function of the time between pulses, Δ t, the source to detector distance, r, and the acoustic wave velocity, c), and I is a generation function describing the source laser pulse characteristics.

In general, it is desirable in materials inspection applications to have a small volume of material under inspection at a given time thus keeping high spatial resolution for flaw detection and such applications. Assuming that the generating laser sources are close together ($R,\ \theta \approx \text{constant}$), that each of the laser source elements is identical, and that the timing is set such that the laser pulses arrive at the detection point simultaneously (ie. $\Delta t_N + \frac{r_N}{c} \approx \text{constant}$) then:

$$\delta_{total} \approx N \frac{1}{R^m} D(\theta) A(t) I \approx N \delta_{single} \tag{3}$$

It is possible therefore to achieve an increase in surface displacement on the order of the number of elements in the array. The gain in detected signal amplitude, η, which may be expected relative to the noise when using a phased array of laser sources is given as:

$$\eta \approx \left(\frac{SNR_{array}}{SNR_{single}}\right)^{\frac{1}{2}} \approx N \tag{4}$$

It is also important to note here that the directivity of the array follows the directivity of the individual elements in the array[16]. In the general case, the increase in surface displacement using an array of laser sources can be calculated with a knowledge of the directivity pattern of the source, source to detector distance, timing of each of the laser pulses, and acoustic wave velocity.

Next consider the case of narrow-band generation of ultrasound where a series of laser pulses arrive at the detection point separated by some temporal spacing, Δ t. Assume that all of the acoustic pulses are generated by identical laser sources at the same point on the specimen. The gain in detected signal amplitude in this case may be given as[17]:

$$\eta = \left(\frac{SNR_{narrowband}}{SNR_{broadband}}\right)^{\frac{1}{2}} = \left(\frac{Noise_{broadband}}{Noise_{narrowband}}\right)^{\frac{1}{2}} \tag{5}$$

The acoustic pulse amplitudes generated by each of the laser pulses in the acoustic pulse train are assumed to be equal. If the detection system is shot noise limited then the noise function is a constant at all frequencies (white noise) and Equation (5) may be simplified as follows:

$$\eta = \left(\frac{Noise_{broadband}}{Noise_{narrowband}}\right)^{\frac{1}{2}} = \left(\frac{\Delta f_{broadband}}{\Delta f_{narrowband}}\right)^{\frac{1}{2}} \tag{6}$$

where Δf is the bandwidth of the broad-band and narrow-band signals respectively. If no filtering is done on the broad-band signal then the bandwidth of the broad-band signal is equal to the bandwidth of the detection system. Ideally, the detection system will be tuned to extend only to frequencies present in the acoustic signal to be detected, in which case the bandwidth of the detection system would be equal to the bandwidth of the broad-band *acoustic* signal. If the noise is not a constant then the noise power must be integrated over the appropriate bandwidth.

From frequency analysis, the line-width at each harmonic of the spectrum of a periodic sequence of pulses is reduced according to:

$$\Delta f_{narrowband} \approx \frac{\Delta f_{broadband}}{N} \tag{7}$$

where N is again the number of pulses in the narrow-band pulse train. Depending on the acoustic pulse shape and the temporal spacing between pulses, a certain number of harmonics will contain significant signal energy and should be filtered using, for example, a comb filter. This gives the final approximation for bandwidth reduction as:

$$\Delta f_{narrowband} \approx h\frac{\Delta f_{broadband}}{N} \tag{8}$$

Where h is the number of harmonics to be filtered. Equation 6 gives the final approximation for gain in signal amplitude for a narrow-band over a broad-band signal as:

$$\eta \approx \left(\frac{N}{h}\right)^{\frac{1}{2}} \tag{9}$$

Therefore, to a first approximation, the gain in detected signal amplitude is directly proportional to the number of elements in the array in the phased array case and is proportional to the square-root of the number of pulses divided by the number of harmonics filtered in the narrow-band case. It appears at first that gains are more readily achieved using phased array rather than narrow-band modulation. It must be noted, however, that there are several advantages of using narrow-band generation even though the gain is smaller than that achieved in the phased array case. First, when generating with a phased array of laser sources, a larger volume of material is interrogated than when generating with a single source or a series of sources hitting the same point (as in the narrow-band case) thus perhaps losing some spatial resolution in the evaluation process. Also for this reason, small defects near the source may interact only with a small portion of the interrogating beam causing limited reflection and attenuation. Next, when using a phased array the specimen thickness or source to detector distance must be known in order to set the necessary temporal delays in the generation of bulk waves. The acoustic wave velocity must be known to calculate this same parameter in the generation of both bulk and surface waves. In practical nondestructive evaluation applications, this information is often not readily available or may be changing with environmental conditions (the change in acoustic wave velocity caused by heating a material, for instance). This information is not needed in the narrow-band case. The narrow-band case has the disadvantage that the detected signal must be filtered in order to match the reduced bandwidth of the generated acoustic signal and care must be taken

during this process to maintain the integrity of the signal. For example, no phase shifts must be introduced if the correct time of arrival of the signal is to be preserved.

Experimental Setup

The experimental arrangement is shown in *Figure 3*. Ten Nd:YAG laser cavities were constructed with each cavity consisting of an end mirror (100% reflector), active Q-switching elements: lithium niobate crystal and polarizer, a pump chamber containing the flashlamp and laser rod (4 x 80mm), and an output coupler (60% reflector). The pump chambers were cooled with forced air and the flashlamps pumped with a single high voltage power supply. The adjustable time delays between laser firings were accomplished with a digital timing circuit which sent individual trigger pulses at a chosen temporal spacing to Q-switch firing circuits associated with each cavity. Note that all of the flashlamps were pumped simultaneously with the cavity in the low-Q state (closed). Then, after a fixed period of time allowing for population inversion in the laser medium, the cavities were switched to the high-Q state (open) one at a time with a fixed delay between the opening of each consecutive cavity. The result was a series of laser pulses which exited the system at frequencies ranging from less than 1 MHz to as high as 20 MHz. A 10 ns variability was observed in the firing time of each laser. The width of the output pulses was approximately 13 ns and the output energy could be adjusted up to 50 mJ. *Figure 4* gives an example of the output of the laser system as detected with an avalanche photodiode when the system was tuned to approximately 400 ns between pulses.

After exiting each cavity, the laser pulses were directed, with adjustable 45 degree laser mirrors, through a focusing lens and onto the specimen of interest. The specimens used were highly polished aluminum disks with thicknesses of 10 and 30 mm. A stabilized Michelson interferometer connected to a digital oscilloscope was used for detection and data acquisition. The waveforms were then transferred to a personal computer for analysis and digital signal processing when appropriate. For surface wave evaluation a cylindrical lens was used to focus the beams to line sources. Generation and detection were done on the same side of the specimen. For the bulk wave setup, a spherical lens was used to generate point sources, and in this case opposite side generation and detection was used.

Results and Discussion

The waveforms shown in this section are the result of single-shot events. No signal averaging has been done. Also, no surface coatings or other surface modifications were applied to the specimens under investigation.

A. Surface Waves

For the surface wave experiments, the laser sources were focused to line sources of approximate dimension 8mm by 0.5mm and the laser energy per pulse was reduced until no signs of ablation were present. This point occurred when the Q-switched pulse energy was approximately 10 mJ per pulse. Note that this gives a power density slightly above the theoretical ablation threshold for aluminum, but the characteristics of the generated Rayleigh waves

combined with the fact that no surface damage was observed after repetitive firing indicate a thermoelastic generation mechanism. The line source dimension given represents an average source size as, owing to the geometry of the setup, there was a slight variability in the source element dimensions. For the phased array case, the illuminating lines were adjusted to a spacing of 0.93 mm and the delay between pulses set to 320 ns. The detection point was placed along the perpendicular bisector of the illuminating line sources, giving the maximum amplitude displacement considering the Rayleigh wave directivity pattern for a line source. The first laser pulse to impinge on the specimen was that farthest away from the detection point; the next laser pulse 0.93 mm closer to the detection point and so on. The center of the array was 19.8 mm from the detection point. The resulting ultrasonic signal was the superposition of the surface waves generated by each of the ten laser line sources. A comparison of surface waves generated with a single laser source and that generated with a ten element phased array is given in *Figure 5*. The single laser source was generated with a laser pulse in the center of the array and was selected for presentation because its peak-to-peak amplitude at the detection point is representative of the average displacements generated by the individual elements of the array. A comparison of the waveforms in *Figures 5a* and *5b* shows a nine-fold increase in the peak-to-peak signal amplitude, while the noise level remains constant. This figure agrees quite well with the previous predictions, noting that the larger geometric losses encountered by the surface waves from the outer elements are counterbalanced by the smaller losses of the closer elements.

For the narrow-band case, all ten elements in the array were focused to line sources at the same point on the specimen and the time between pulses was set to 360 ns. The source to detector distance was 20 mm. The resulting waveform is shown in *Figure 6a*. *Figure 6b* shows how the acoustic signal energy is centered around the pulse repetition frequency, 2.8 MHz. Note that there is very little acoustic energy at the harmonics of the repetition frequency. This is the case because the temporal spacing between pulses was chosen such the generated surface waves "tied together" forming a tone burst at nearly a pure frequency thus eliminating the presence of harmonics. This allows one to use a simple band-pass filter to achieve the desired increase in sensitivity as is shown in *Figure 6c*. The width of the filter pass-band was 1.4 MHz. In this case the increase in $SNR_{amplitude}$ appears to be greater that the 3.2 predicted by Equation (9) with h=1. This was the result of the fact that the waveform depicted in *Figure 6a* was detected with a high fidelity interferometer with a bandwidth of 50 MHz. This frequency range extends well outside the bandwidth of the acoustic signal. Thus the actual gain in detected signal amplitude can be found through Equation (6), with a broadband bandwidth of 50 MHz and a narrow-band bandwidth of 1.4 MHz, to be approximately 5.9 which agrees well with the *Figure 6*.

B. Bulk Waves

For the phased array setup a 10 mm thick aluminum specimen was used, and in all of the bulk wave cases opposite side generation and detection was used. The laser pulses were focused to spot sizes of 2.6 mm diameter (again the spot sizes varied slightly) with a spherical lens and the pulse energy was reduced to approximately 10 mJ. The time between pulses was set to 100 ns. The laser pulses were set such that the center of the array was 42 degrees off of epicenter. The angles off epicenter of the generating laser pulses ranged from 52 degrees for the first arriving laser pulse to 21 degrees for the last arriving laser pulse. The spatial and temporal parameters

were set such that all of the longitudinal waves arrived at the detection point simultaneously. Due to the large angular spread of the generating sources, the assumptions made when deriving Equation (3) are not valid. The angle off of epicenter, θ , and the propagation distance, R, are not constant for each of the generating elements. Taking into account the far-field directivity pattern for longitudinal waves[1] in aluminum and the spherical propagation factor, an estimate for the relative acoustic amplitudes projected normal to the sample surface from each wave generated may be given as

$$\delta \propto \left(\frac{1}{R}\right)\left(\frac{2\sin(2\theta)\sin(\theta)(k^2-\sin^2\theta)^{\frac{1}{2}}}{(k^2-2\sin^2\theta)^2+4\sin^2\theta(1-\sin^2\theta)^{\frac{1}{2}}(k^2-\sin^2\theta)^{\frac{1}{2}}}\right)(\cos\theta) \quad (10)$$

where R is the source to detector distance, θ is the angle off of epicenter, and k can be related to the longitudinal (c_1)and shear wave (c_2) velocities as follows

$$k = \frac{c_1}{c_2} \quad (11)$$

The normalized acoustic wave amplitudes expected from each array element is presented in *Figure* 7. This indicates that the displacements produced by the center elements should be the largest with slightly lower amplitude displacements produced by the outer elements. *Figure 8* shows the results of this experiment with waveforms generated with two element (a), five element (b), and ten element (c) arrays. The two element array shows the elastic waves generated with elements 4 and 5 while the five element array shows the waves generated with elements 3-7. The gain in detected signal amplitude of the longitudinal wave for the five and ten element arrays over the two element array was predicted to be 2.47 and 4.42 respectively. The experimentally measured gain was found to be 2.12 for the five element array and 4.68 for the ten element array relative to the two element array. Note that detection of the longitudinal arrival with a single laser source proved difficult at such low power densities.

In the narrow-band case, all of the beams from the laser source were focused to a single element on the specimen (the pulse characteristics the same as given above) and the time between pulses was set to 360 ns. The clearest example of increasing the SNR through bandwidth reduction was that using a 30 mm thick aluminum specimen and a signal detection angle of 24 degrees off of epicenter. This angle was chosen to ensure comparable displacement contributions from the shear and longitudinal wave modes. *Figure 9a* shows the signal as detected with the interferometer with no filtering done. *Figure 9b* shows the result of lowpass filtering *Figure 9a* at 10 MHz, which is approximately the bandwidth limit of an acoustic event generated by a single element in the array. *Figure 9c* shows the result of filtering *Figure 9a* with a comb filter at 2.8 and 5.6 MHz. with a total bandwidth of approximately 1.5 MHz. Three distinct wave packets are present and are explained as follows: 1) electronic noise from the firing of the laser Q-switches, 2) arrival of the longitudinal pulse train, and 3) arrival of the shear pulse train. From Equation (6), a 2.6 fold increase in $SNR_{amplitude}$ would be expected in *Figure 9c* over *Figure 9b*. Qualitatively, it appears that the increase is somewhat greater than predicted. This may indicate that the noise present in the signal is not actually constant at all frequencies (white noise) and that by

introducing the narrow comb filter some other noise sources present in the 10 MHz bandwidth of *Figure 9b* are eliminated.

Conclusion

A ten cavity laser system was designed to provide control of the timing between laser pulses, spatial modulation of the pulses on the surface of a specimen, and output pulse energy necessary for a detailed study of pulsed laser array generation of ultrasound. The increase in sensitivity seen in the experimental results agrees well with the theoretical predictions in both the narrow-band and phased array cases. The increase in detected signal amplitude is proportional to the number of elements in the array in the phased array case and proportional to the square-root of the number of elements in the array divided by the number of harmonics to be filtered in the narrow-band case. It is important to emphasize that the experimental results given were generated in the thermoelastic regime without the aid of any surface coatings. Laser ultrasonic systems using an array of laser sources to generate narrow-band or phased acoustic waves, together with improvements in the sensitivity of optical detection systems, should help to make laser ultrasonics a more practical option for many industrial inspection and materials characterization applications.

This work was supported in part by the U.S. Air Force Wright Laboratories.

References

1. **Scruby, C.B. and Drain, L.E.** *Laser Ultrasonics: Techniques and Applications,* Adam Hilger, Bristol, Philadelphia, and New York (1990).

2. **Aussel, J.D., LeBrun, A., Baboux, J.C.** Generating Acoustic Waves by Laser: Theoretical and Experimental Study of the Emission Source, *Ultrasonics*, **26**, 245-255 (1988).

3. **Mckie, A.D.W., Liao, T., Ryang, H., Addison, R.C.** Laser-based ultrasonics-applications to NDE and process monitoring, in: *Proc. IEEE Ultrasonics Symposium* V2, 641-649 (1993).

4. **Monchalin, J.P.** Optical detection of ultrasound at a distance using a confocal Fabry-Perot interferometer, *Appl. Phys. Lett.* **47**(1), 14-16 (1985).

5. **Hutchens, D.A., Dewhurst, R.J., Palmer, S.B.** Laser generated ultrasound at modified metal surfaces *Ultrasonics*, **6**, 103-108 (1981).

6. **Addison Jr, R.C., Graham, L.J., Linebarger, R.S., and Tittmann, B.R.** Laser-based ultrasonics for the inspection of solids, in: *Review of Progress in Quantitative Non-Destructive Evaluation* Vol 7A (Eds. Thompson, D.O. and Chimenti, D.E.) Plenum Press, New York, 585-594 (1988).

7. **Huang, J., Krishnaswami, S., Achenbach, J.D.** Laser generation of narrow-band surface waves *J. Acoust. Soc. Am.*, **92**(5), 2527-2531 (1992).

8. **Mckie, A.D.W., Wagner, J.W., Spicer, J.B., Penny, C.M.** Laser generation of narrow-band and directed ultrasound *Ultrasonics*, **27**, 323-330 (1989).

9. **Edwards, C., Buschell, A.C., Palmer, S.B., Nakano, H.** Laser interference grating for surface wave generation *Nondestr. Test. Eval.*, **10**, 15-23 (1992).

10. **Wagner, J.W., Deaton, J.B. Jr., Spicer, J.B.** Generation of ultrasound by repetitively Q-switching a pulsed Nd:YAG laser Applied Optics , **27**(22), 4696-4700 (1988).

11. **Deaton, J.B. Jr., Mckie, A.D.W., Spicer, J.B., Wagner, J.W.** Generation of ultrasound with a long cavity mode-locked Nd:YAG laser Appl. Phys. Lett., **56**, 2390-2392 (1990).

12. **Yang, J., DeRider, N., Ume, C., Jarzynski, J.** Non-contact optical fiber phased array generation of ultrasound for non-destructive evaluation of materials and processes, *Ultrasonics*, **31**(6), 387-394 (1993).

13. **Noroy, M-H., Royer, D., Fink, M.** The laser-generated ultrasonic phased array: Analysis and experiments, *J. Acoust. Soc. Am.*, **94**(4), 1934-1943 (1993).

14. **Steckenrider, J.S., Murray, T.W., Deaton, J.B. Jr., Wagner, J.W.** Sensitivity enhancement in laser ultrasonics using a versatile laser array system, *J. Acoust. Soc. Am.*, in press.

15. **Wagner, J.W. and Spicer, J.B.** Theoretical noise-limited sensitivity of classical interferometery, *J. Optical Society of America*, **4**, 1316-1326 (1987).

16. **Wagner, J.W., McKie, A.D.W., Spicer, J.B., Deaton Jr., J.B.** Modulated laser array sources for the generation of narrowband and directed ultrasound, *J. Nondes. Eval.*, **9**(4), 263-270 (1990).

17. **Berthelot, Y.** Thermoacoustic generation of narrow-band signals with high repetition rate pulsed lasers, *J. Acoust. Soc. Am.*, **85**(3), 1173-1181 (1989).

Figure 1 Phased array of laser sources. The spatial and temporal laser pulse parameters are chosen such that wavefront superposition occurs at the detection point.

Figure 2 Narrow-band generation of acoustic waves.

Figure 3 Experimental setup used for the generation of narrow-band ultrasonic signals and phased array single pulses.

Figure 4 Laser system output as detected with an avalanche photodiode with the pulse separation set to 400ns.

Figure 5 Surface waves generated with a) a single laser source and b) a ten laser array with spatial and temporal parameters chosen such that superposition of the waves generated with each source occurred.

Figure 6 a) narrow-band surface waves generated with an array of laser sources b) the power density spectrum of waveform (a) and c) waveform (a) after bandpass filtering at 2.6 MHz.

Figure 7 Normalized longitudinal wave amplitudes expected from each generation element in the array.

Figure 8 Bulk waves generated with a) two laser sources b) a five element array and c) a ten element array. The spatial and temporal parameters of the generating pulses were chosen such that superposition of the longitudinal waves generated with each source occurred.

Figure 9 Narrow-band bulk waves generated in a 30mm Al specimen showing a) raw signal as detected with interferometer b) signal after low-pass filtering at 10 MHz and c) signal after comb filtering at 2.8 and 5.6 MHz. The numbers on waveform (c) indicate the firing of the Q-

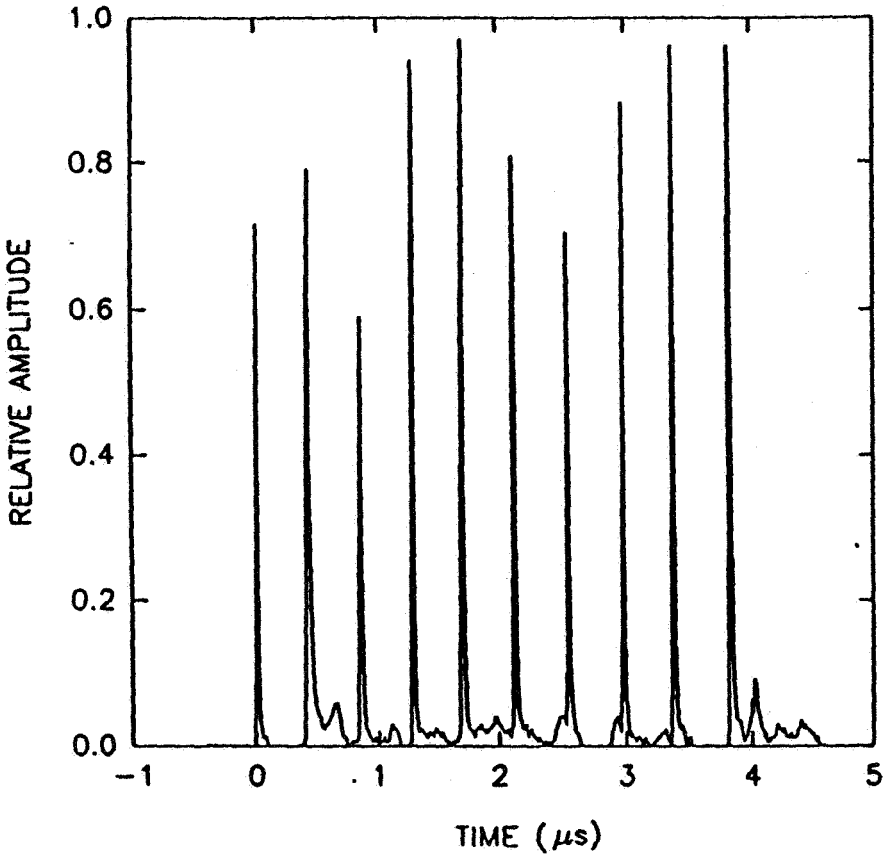
1.0
0.8
0.6
0.4
0.2
0.0
RELATIVE AMPLITUDE
−1
0
1
2
3
4
5
TIME (μs)

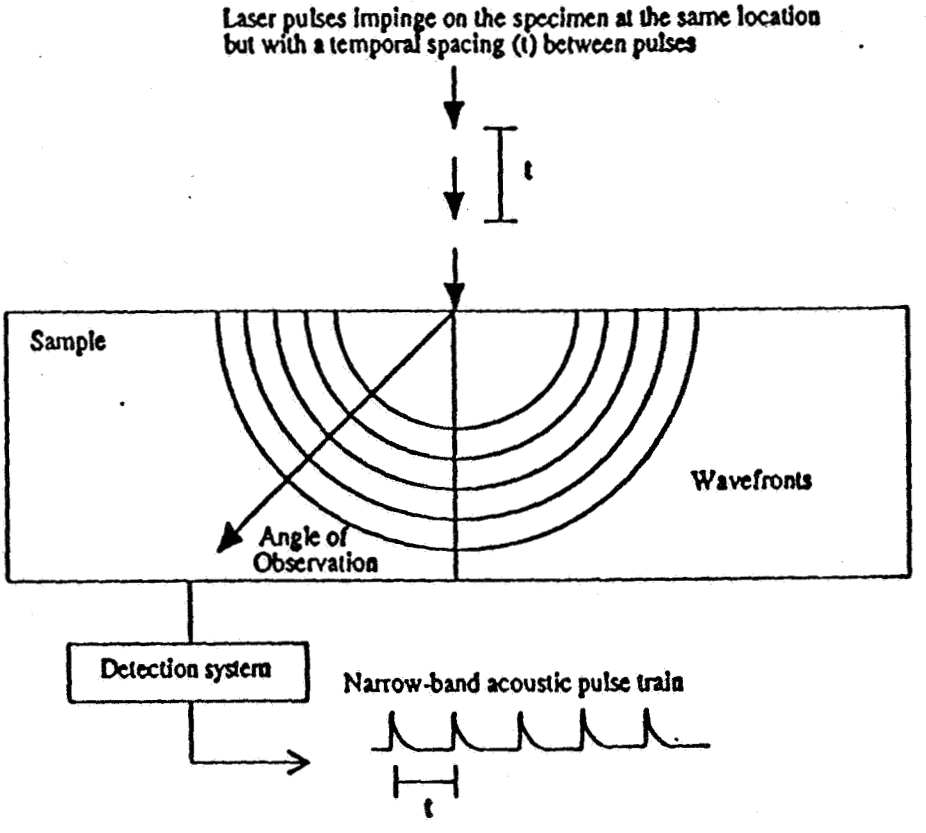
Laser pulses impinge on the specimen at the same location but with a temporal spacing (t) between pulses
t
Sample
Wavefronts
Angle of Observation
Detection system
Narrow-band acoustic pulse train
t

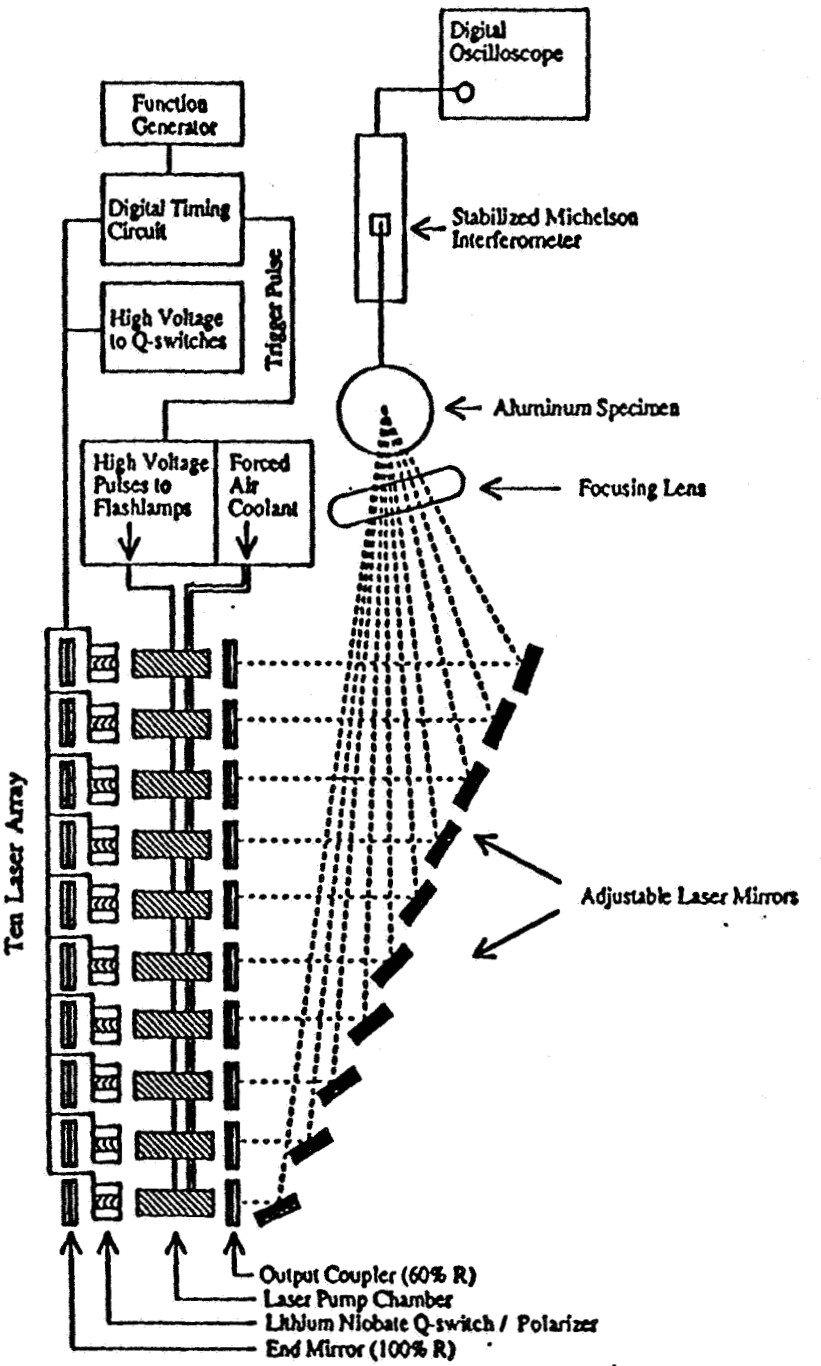
Digital Oscilloscope
Function Generator
Digital Timing Circuit
High Voltage to Q-switches
Trigger Pulse
Stabilized Michelson Interferometer
Aluminum Specimen
High Voltage Pulses to Flashlamps
Forced Air Coolant
Focusing Lens
Ten Laser Array
Adjustable Laser Mirrors
Output Coupler (60% R)
Laser Pump Chamber
Lithium Niobate Q-switch / Polarizer
End Mirror (100% R)

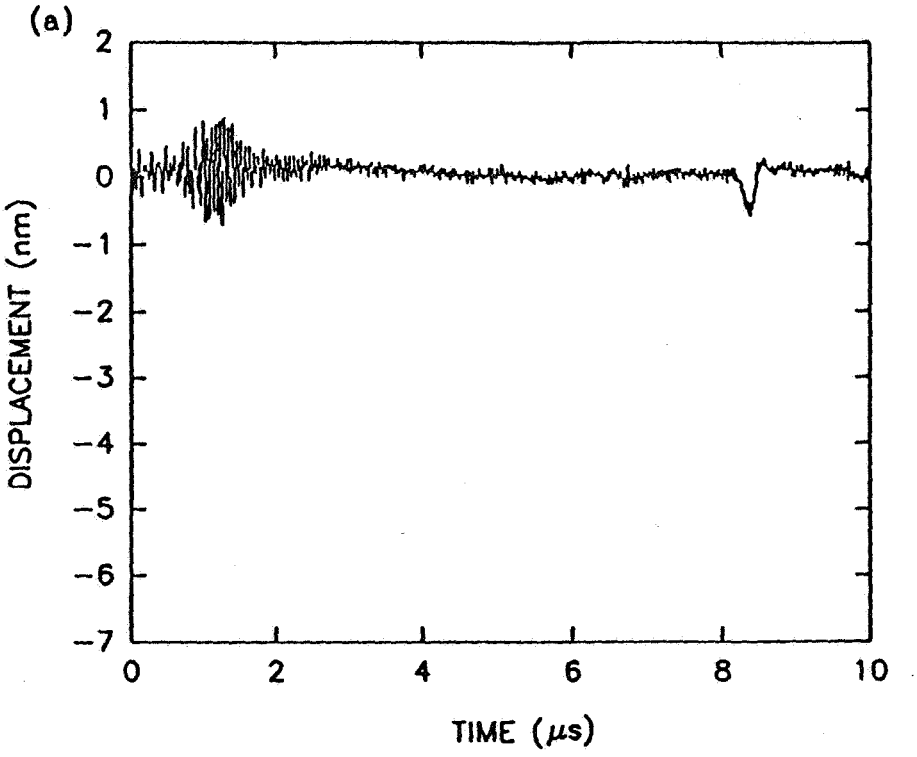
(a)
DISPLACEMENT (nm)
2
1
0
−1
−2
−3
−4
−5
−6
−7
0
2
4
6
8
10
TIME (μs)

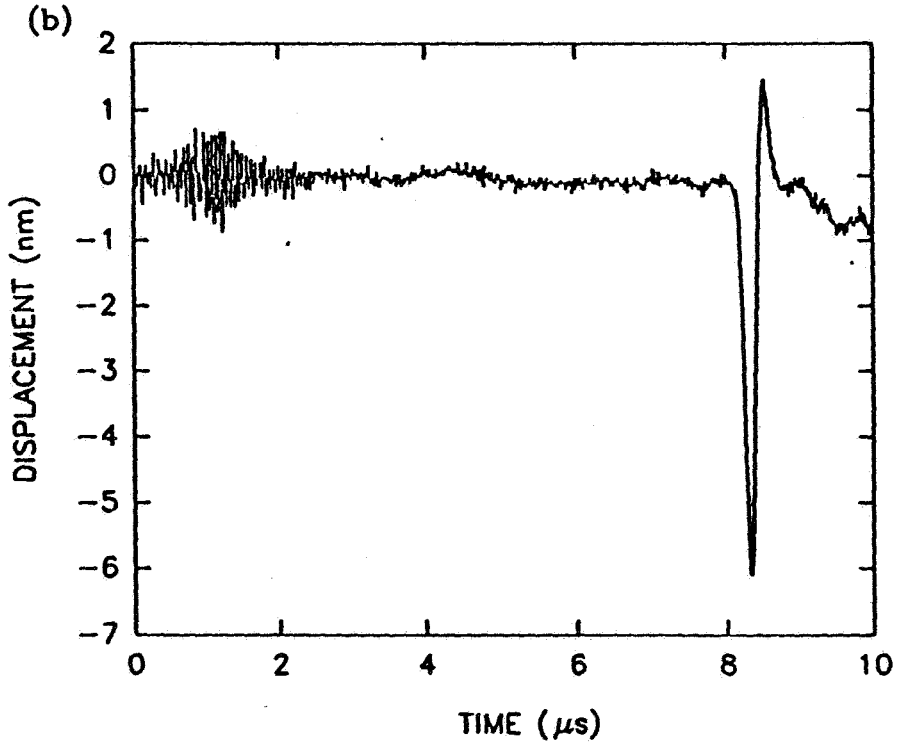
(b)
DISPLACEMENT (nm)
2
1
0
−1
−2
−3
−4
−5
−6
−7
0
2
4
6
8
10
TIME (μs)

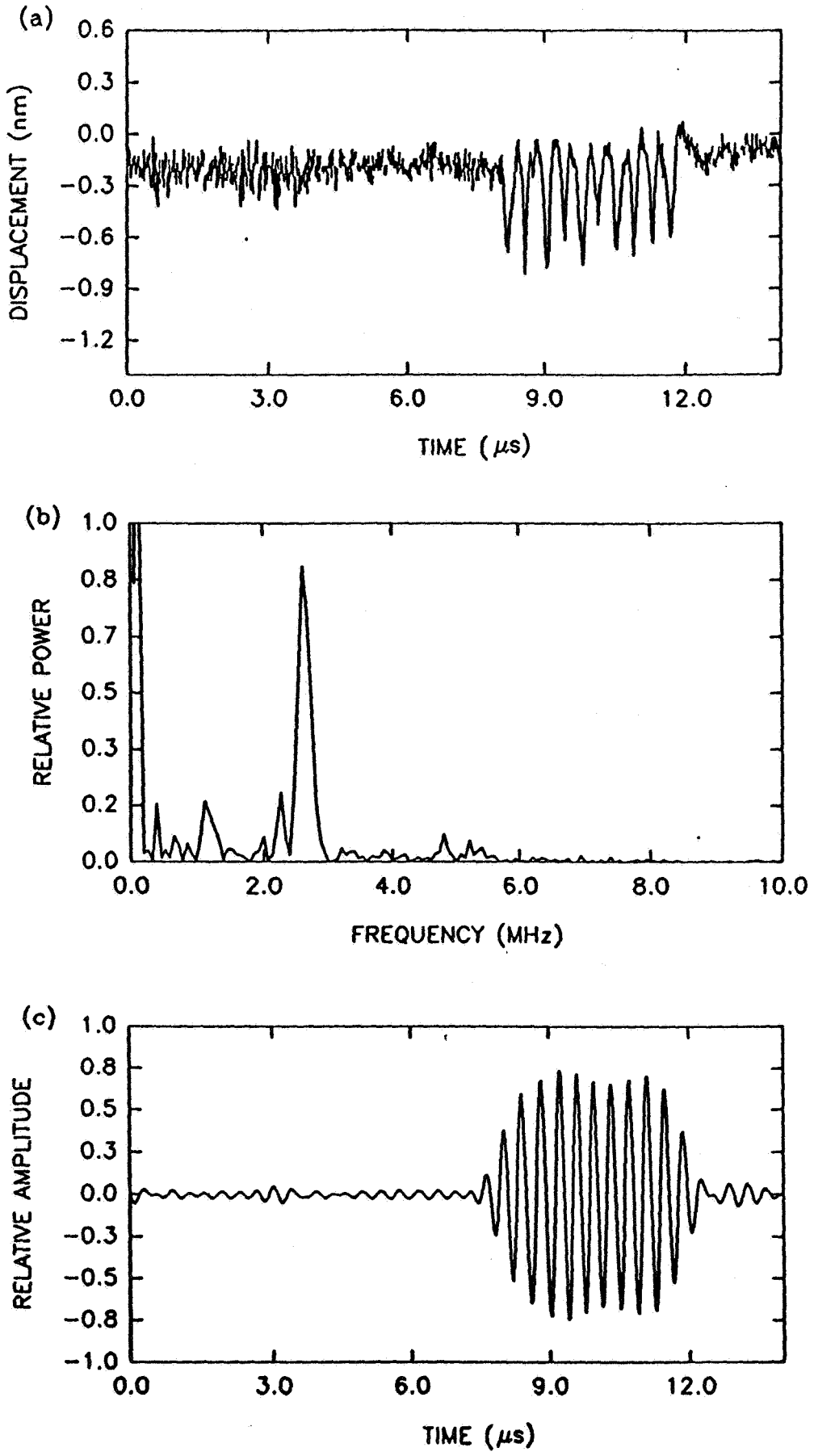
(a)
DISPLACEMENT (nm)
0.6
0.3
0.0
−0.3
−0.6
−0.9
−1.2
0.0
3.0
6.0
9.0
12.0
TIME (μs)
(b)
RELATIVE POWER
1.0
0.8
0.7
0.5
0.3
0.2
0.0
0.0
2.0
4.0
6.0
8.0
10.0
FREQUENCY (MHz)
(c)
RELATIVE AMPLITUDE
1.0
0.8
0.5
0.3
0.0
−0.3
−0.5
−0.8
−1.0
0.0
3.0
6.0
9.0
12.0
TIME (μs)

Relative Acoustic Amplitudes

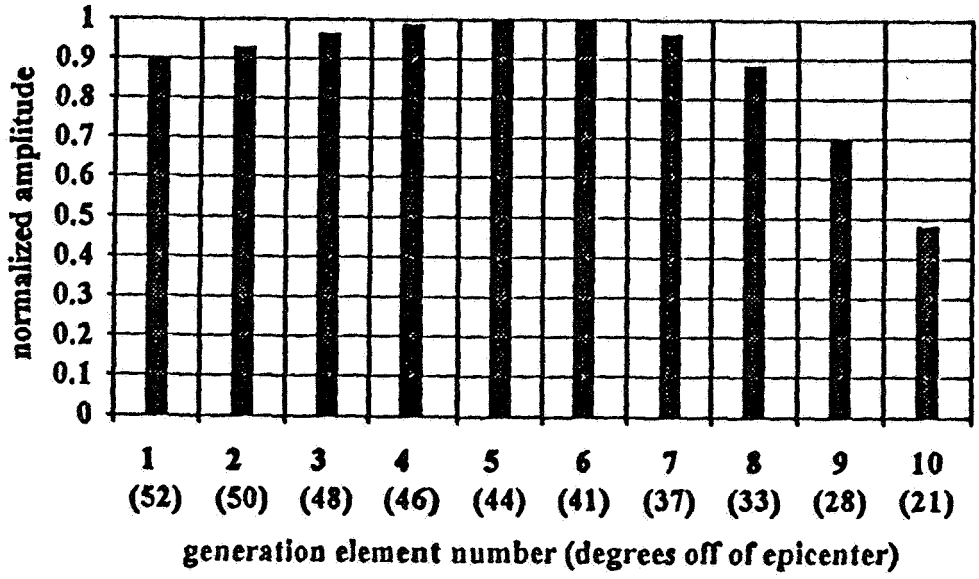

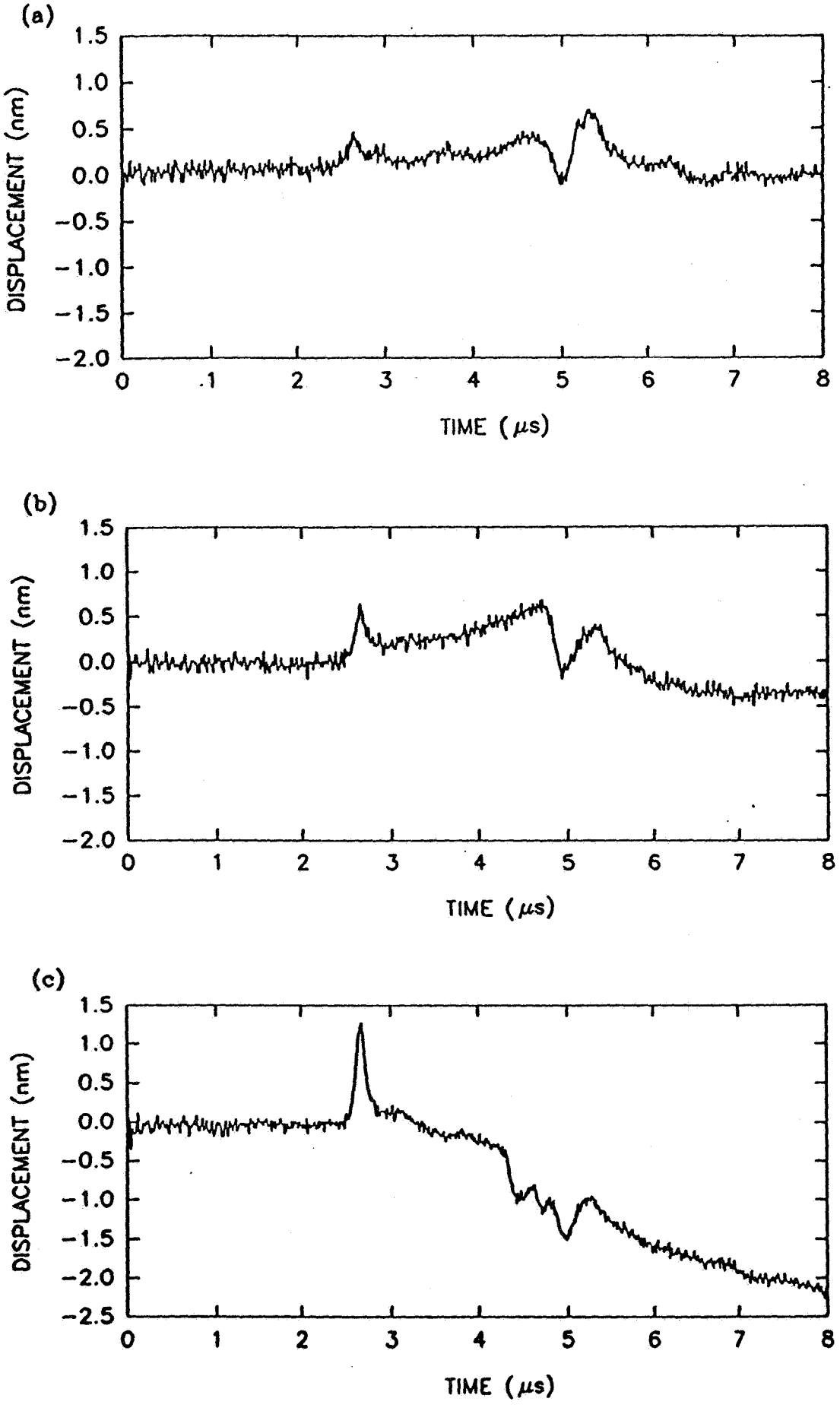
(a)
DISPLACEMENT (nm)
1.5
1.0
0.5
0.0
−0.5
−1.0
−1.5
−2.0
0
.1
2
3
4
5
6
7
8
TIME (μs)
(b)
DISPLACEMENT (nm)
1.5
1.0
0.5
0.0
−0.5
−1.0
−1.5
−2.0
0
1
2
3
4
5
6
7
8
TIME (μs)
(c)
DISPLACEMENT (nm)
1.5
1.0
0.5
0.0
−0.5
−1.0
−1.5
−2.0
−2.5
0
1
2
3
4
5
6
7
8
TIME (μs)

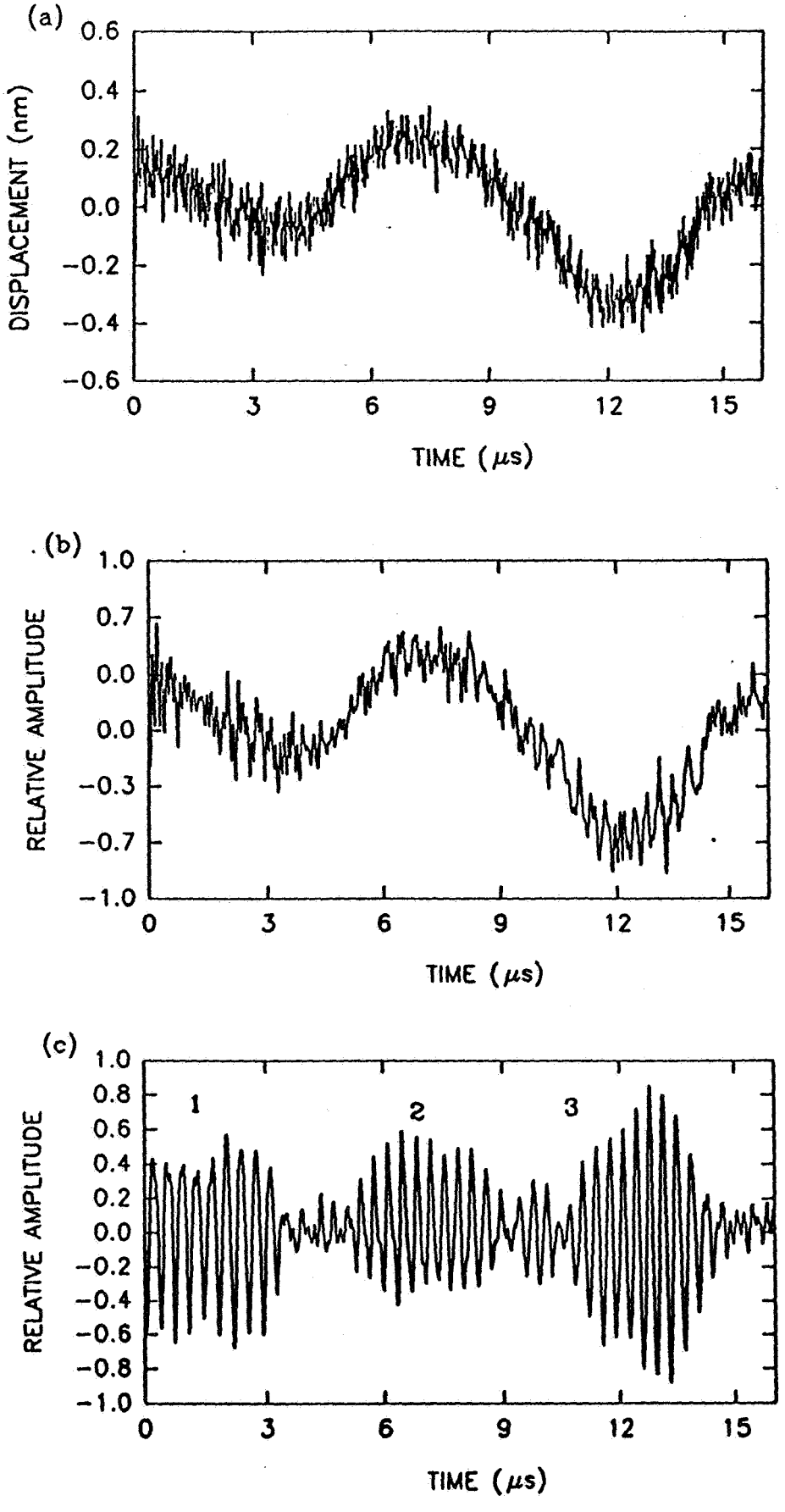
(a)
DISPLACEMENT (nm)
0.6
0.4
0.2
0.0
−0.2
−0.4
−0.6
0
3
6
9
12
15
TIME (μs)
(b)
RELATIVE AMPLITUDE
1.0
0.7
0.0
0.0
−0.3
−0.7
−1.0
0
3
6
9
12
15
TIME (μs)
(c)
RELATIVE AMPLITUDE
1.0
0.8
0.6
0.4
0.2
0.0
−0.2
−0.4
−0.6
−0.8
−1.0
1
2
3
0
3
6
9
12
15
TIME (μs)

II: THE INTERFEROMETRIC DETECTION OF ULTRAFAST PULSES OF LASER GENERATED ULTRASOUND

(From the PhD Dissertation of C. J. Fiedler, 1996)

1. Introduction

A novel technique to measure nondestructively the thickness and properties of thin coatings has been developed. High frequency pulses of ultrasound were generated in a coating using ultrafast (100 fs) pulses of laser light. These ultrasonic pulses were used to inspect thin coatings (30 nm - 500 nm) in a pulse-echo mode. The ultrasonic echoes were detected using an innovative delay line based pulsed interferometer.

The principle of operation of this technique takes advantage of the fact that short pulses of laser light cause rapid heating of a metallic coating which in turn, through thermal expansion, causes an elastic pulse to propagate through the film. As with conventional ultrasonics, it is possible to determine elastic parameters of materials and physical dimensions based on the time of flight of such an elastic pulse. To make time of flight measurements in very thin films, the pulses themselves must be extremely short. Using a mode locked Ti:Sapphire laser, pulses on the order 100 fs can be used to generate correspondingly short elastic pulses. Longer optical pulses on the order of nanoseconds have been used for conventional laser ultrasonics, but for use in thin films, such long pulses would have physical pulse widths many times the film thickness.

Once a short elastic pulse propagates through a film coating to the coating/substrate interface and returns again surface to film, it is necessary to detect its arrival. In recent years, investigators have used the fact that small strains introduced at the surface of the film when a stress wave arrives causes a minute change in the complex refractive index and, thus, the reflectivity of the film surface. Thus, a piezoreflective method can be used in some materials to detect the arrival of the stress wave. Not all materials exhibit large piezoreflective effects, however. Consequently, alternative detection techniques have been considered. In this work, a pulsed interferometer system was employed based on a time delay configuration. The interferometer is a dual point and, therefore, differential interferometer which measures the relative change in surface displacement at one point on the film relative to a second point a few millimeters away. The interferometer uses a portion of the same pulse beam from the Ti:Sapphire laser used to generate the sound. However, a time difference between the generation of the sound and the introduction of the laser pulse into the interferometer is accomplished through the use of a variable optical pulse delay in the heating beam as shown in Figure 1. Lock-in detection of the fluctuations in the interferometer signal as a function of path difference between the heating and sensing beams permits sensitive detection of the arrival of ultra short elastic waves with effective frequency bandwidths in excess of 100 GHz.

The thicknesses of a 25 nm thick gold coating, a 67 nm thick aluminum coating, and a 170 nm thick molybdenum coating were measured using ultrasonic echoes. The frequency spectrum of the echoes from the gold coating extended up to 100 GHz for displacements as small

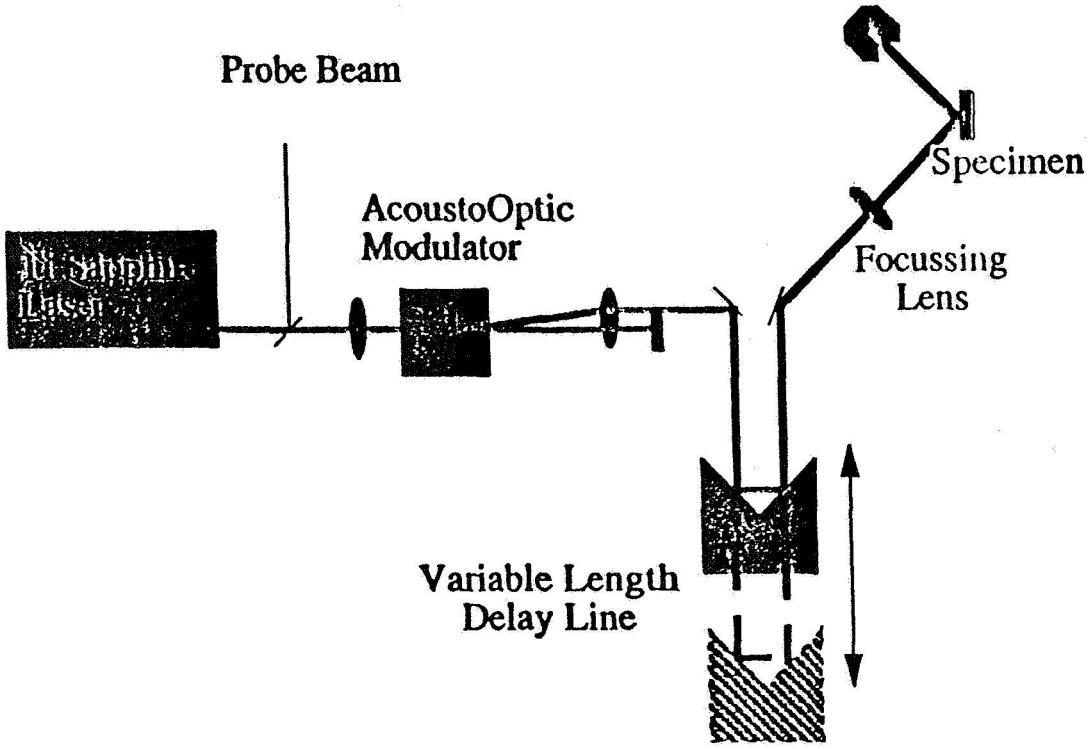

Figure 1: Heating Beam Schematic

as 4 pm. Piezoreflective detection of ultrasonic echoes as demonstrated by other investigators verified the data for the aluminum coating but only the interferometric technique gave useful results on the gold and molybdenum coatings.

Models for the absorption of the laser pulse, the generation of ultrasound, the propagation and attenuation of ultrasound due to losses upon reflection, the displacement of the surface of the specimen due to ultrasound, interferometric and piezoreflective detection, and thermal wave generation and detection were developed and validated. For a molybdenum coating, the displacement of the specimen surface due to thermal waves was predicted to within 3%, the displacement due to the absorption of the heating pulse was predicted to within 12%, and the displacement due to the ultrasonic echoes was predicted to within 5 pm.

2. Experimental Configuration

2.1 The Heating Beam

2.1.1 Ti:Sapphire Laser

A Ti:Sapphire laser pumped with a Spectra Physics BeamLok 2080-12W Argon Ion laser was purchased through this program. The Argon Ion laser produced 20 watts of power but was operated at 8 watts because it produced the optimal Ti:Sapphire laser beam quality.

The Ti:Sapphire laser was a Spectra Physics Tsunami Model 3960-L1S, operated with the standard optics set in the femtosecond mode. The laser had a repetition rate of 82 MHZ and less than 2% noise on the laser beam from 10 Hz to 2 MHZ. The laser beam was less than 2 mm in diameter ($1/e^2$ points) and exited the laser vertically polarized. The wavelength of light produced by the laser could be varied between 710 nm to 850 nm, and the pulse length varied by changing the amount of dispersive glass in the laser cavity. The data reported here were acquired with the Ti:Sapphire laser generating 1.5 watts of average power at 760 nm and a pulse length between 100 and 120 fs.

2.1.2 Acousto-Optic Modulator

An Acousto-Optic Modulator (AOM) was used to chop the heating beam at frequencies ranging from 10 Hz to 10 MHZ. The AOM was a NEOS 35085-3 AOM driven with a NEOS N310815 driver. To chop at frequencies about 1 MHZ, it was necessary to focus the laser beam as it passed through the AOM. Focusing the beam, however, reduced the efficiency of the AOM because the light is no longer collimated as it passes through the AOM. A 400 mm focal length lens was used to allow the chopping frequency to go up to 10 MHZ while maximizing the. efficiency of the AOM. The efficiency of the AOM dropped to 50% which gave an average optical power at the specimen of 250 mW.

2.1.3 Delay Line

The delay line consisted of a CVI 63.5 mm diameter retroreflector with gold mirrors mounted on an Aerotech ATS6000 translation stage. The laser beam reflected off three mirrors in the retroreflector which each had 90% reflectivity.

2.1.4 Heating Beam Focusing

The heating beam was focused onto the specimen using a 125 mm focal length lens. The diameter of the heating beam on the specimen is calculated from:

$$w_0 = \frac{4\lambda f}{\Pi D}$$

The beam waist at the specimen was 60 μm, and the area of the beam on the specimen is 2.827 x 10^{-9} m^2.

The energy per pulse and the average instantaneous power of the laser to the specimen could be calculated from the fact that the average power at the specimen is 0.2 W and the repetition rate of the laser is 82 MHZ. Thus, the unchopped laser beam had an average power of 0.4 W (50% duty cycle) so that each laser pulse had an energy of 4.87 nJ. The instantaneous power for a 100 fs pulse was 48.7 kW, and the instantaneous power density was 1.69 x 10^{13} W/m^2.

2.2 Probe Beam

The probe beam, which is split off the heating beam, is shown schematically in Figure 2.

2.2.1 Optics

The 100 fs pulses of light are so short in time that they are composed of a broad range of wavelengths (due to the Hiesenberg uncertainty principle). Because the pulses are not monochromatic, they are subject to broadening due to dispersion. Reflecting these pulses off conventional multilayer broad band dielectric mirrors can lengthen the pulses from 100 fs to 200 fs. To prevent pulse broadening, single layer Ti:Sapphire mirrors from CVI optics (PTS-767-2037-45-S) were used to preserve the beam quality.

2.2.2 Polarization Sensitive Detection

One of the standard checks to ensure that the experiment was operating properly was to block the probe beam and verify that the lock-in signal goes to zero. On a number of specimens with rough surfaces, it was found that there was still a significant signal even though the probe beam was blocked. After much experimentation, it was determined that, because the changes in reflectivity that the experiment detects are so small, even a little bit of heating beam scattered into the probe beam path by the specimen will generate a significant signal at the photodetector.

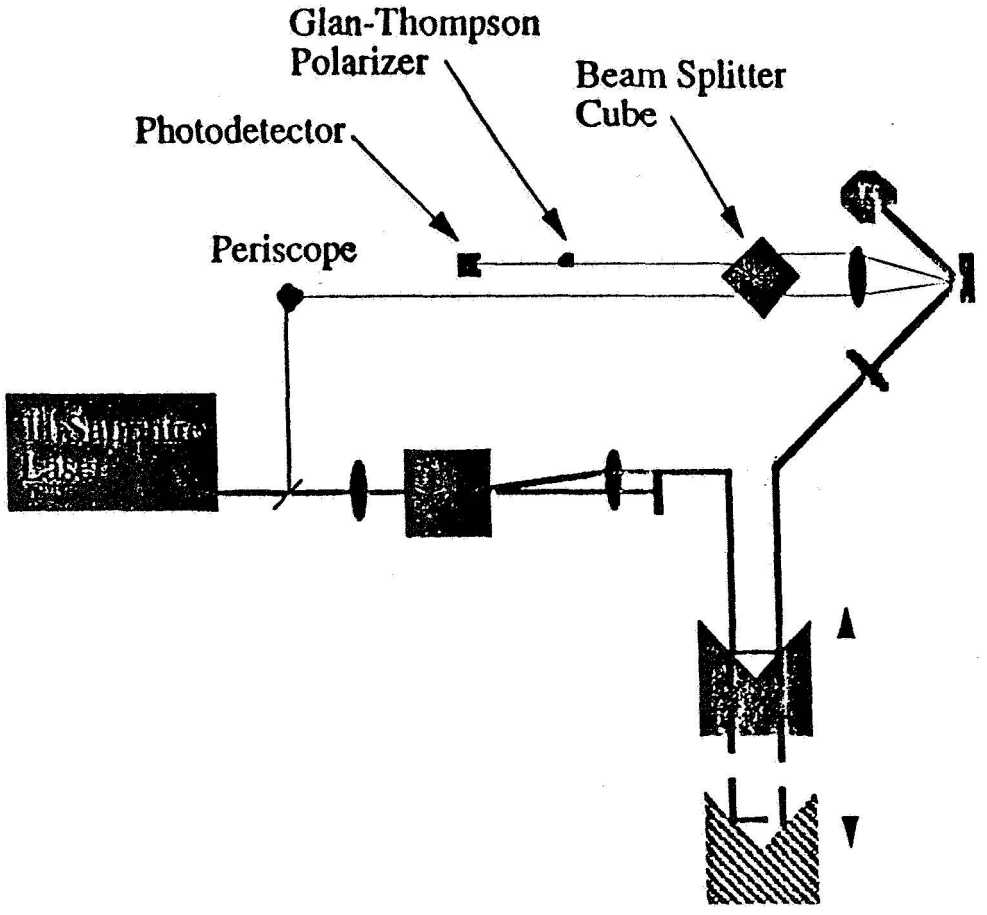

Figure 2: Probe Beam Path

Polarization sensitive detection was used to ameliorate this problem. The laser beam exists the laser vertically polarized. A periscope (see Figure 2) was used to rotate the polarization of the probe beam. The light reflected off the specimen was then directed through a Glan-Thompson polarizer. The polarizer let the horizontally polarized probe beam light pass on to the photodetector while blocking scattered heating beam light with an extinction ratio of 10,000 to 1.

2.3 The Interferometer

The interferometer, shown schematically in Figure 3, is based on a 50/50 non-polarizing beam splitter cube. Light enters the beam splitter cube (the thin line) and is split at the interface into two beams. Each beam travels through the focusing lens to the specimen and then reflects back to the beam splitter cube. Light from each path then interferes with light from the other path (the heavy lines in Figure 3).

Since the laser beam is incident normal to the face of the beam splitter cube, it is acting as a 60/40 beam splitter instead of a 50/50 beam splitter. When the beams recombine at the interface, the same effect happens so that one of the two sets of interfering beams from the beam splitter cube always has complete extinction of the fringes and the other never has complete extinction.

To set up the interferometer, it was necessary to start with the incident laser beam parallel to the dielectric interface. When the two beams emerged from the beam splitter cube, the lens focused them onto the same spot on the specimen.

It was necessary to separate where these beams hit the specimen so that the heating beam can be focused onto only one of the spots. There are a number of ways to separate the beams. The tilt angle of the lens can be adjusted, the beam splitter cube can be rotated, or the angle of the beam incident upon the beam splitter cube can be varied. The problem is, if the wrong adjustment is made, the laser beams will only interfere at a single point along the beam path. A spreadsheet based ray tracing analysis demonstrated that if only the angle of the incoming laser beam to the beam splitter cube is adjusted, the laser beams will continue to interfere along their entire length.

2.3.1 Photodetector

The probe beam light is detected using a New Focus 1801 DC to 125 MHZ amplified photodetector. The photodetector has a $2.4 \times 10^4 \frac{V}{W}$ conversion gain, and a noise equivalent power of $3.3 \frac{pW}{\sqrt{Hz}}$.

2.3.2 Lock-in Detection

The lock-in extender transforms high frequency signals (up to 10 MHZ) down to 1 kHz so that the magnitude and phase of the signal can be measured with a conventional lock-in amplifier. A Palo Alto Research Corporation PAR100 Lock-in Extender was used for the experiments in this thesis and was typically used with a gain of 40 db (Figure 4).

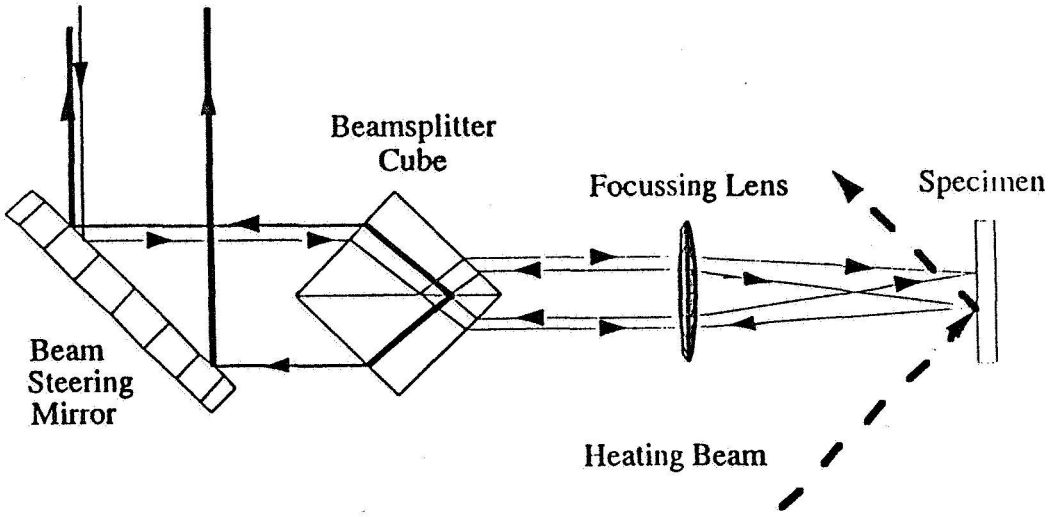

Figure 3: Schematic showing the Ultrafast Pulsed Interferometer

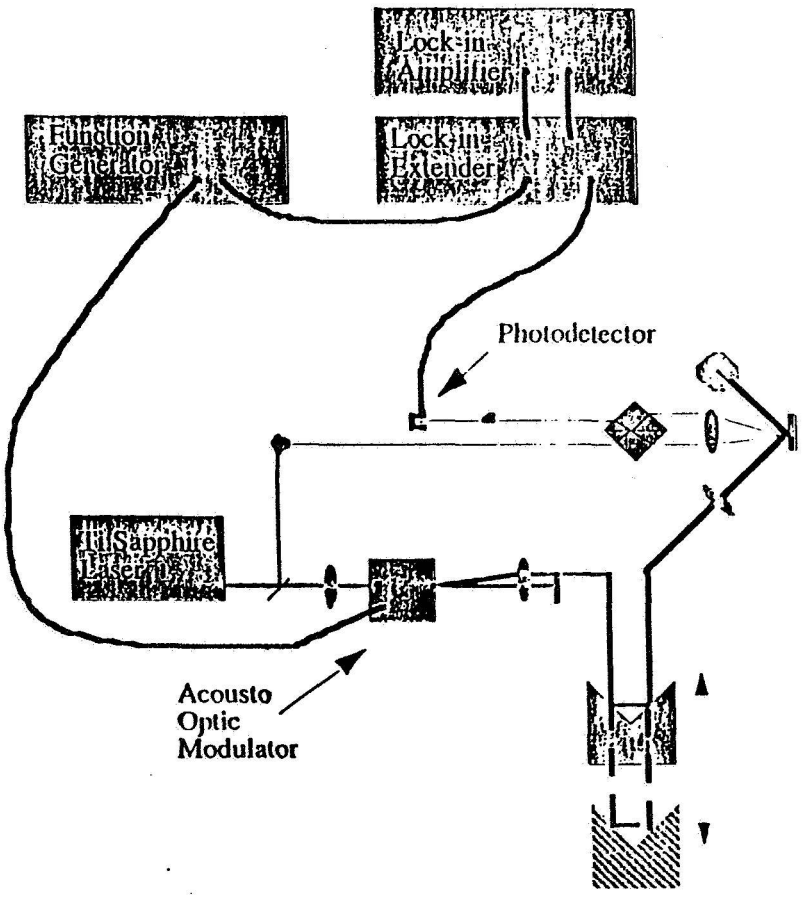

Figure 4: Instrumentation Schematic

2.3.3 Tilt Scans

The relative phase difference between the arms of a conventional interferometer can be varied by changing position of the reference mirror. This is accomplished by tilting the specimen. By varying this tilt, it should be possible to generate the classic interference signals.

A Stanford Research Systems SRS530 lock-in amplifier was used to measure the magnitude and phase of the signals coming from the lock-in extender.

3. Data Acquisition

The entire experiment was automated, allowing all important parameters of the experiment (chopping frequency, translation stage movement, and interferometric/piezoreflective beam block) to be controlled automatically and the data from the lock-in amplifier and volmeter to be collected via the computer. The instrumentation in the experiment was interfaced to a Macintosh computer using an IEEE 488 instrumentation bus. The programs to control the experiment and acquire data were written using Labview, an icon based data acquisition programming language developed by National Instruments, Inc.

All the plots and many of the models for this research were produced using Igor, a plotting package written by Wavemetrics. In addition to a wide range of plotting features, Igor has a programming language which automates repetitive plotting tasks. The programming language was also used to model the data so that the model could be compared directly to the experimental data. Igor reduced the time to plot the experimental data from the multiple tilt scans from over an hour to a few minutes.

4. Experimental Results

4.1 Interferometer with Piezoelectric Excitation

Interferometers capable of resolving picometers of displacement have been constructed[1] and pulsed interferometers have been constructed[2], but no known interferometer using Ti:Sapphire ultrafast pulses has been reported. To demonstrate that interferometry is possible with Ti:Sapphire pulses, the interferometer was first tested on a specimen which was excited with a conventional piezoelectric transducer. The experimental configuration showing the transducer located to excite only the signal beam of the interferometer is shown in Figure 5.

The piezoelectric transducer was a 1 MHZ, 0.5 inch diameter Panametrics transducer which was designed to be used with polystyrene wedges. The specimen was a glass microscope slide coated with a thick coating (approximately 600 μm) of aluminum. The transducer was placed in a jig which pressed it against the microscope slide, and honey was used to couple the longitudinal waves from the transducer into the slide. The transducer was excited with a 1 MHZ sine wave from the function generator.

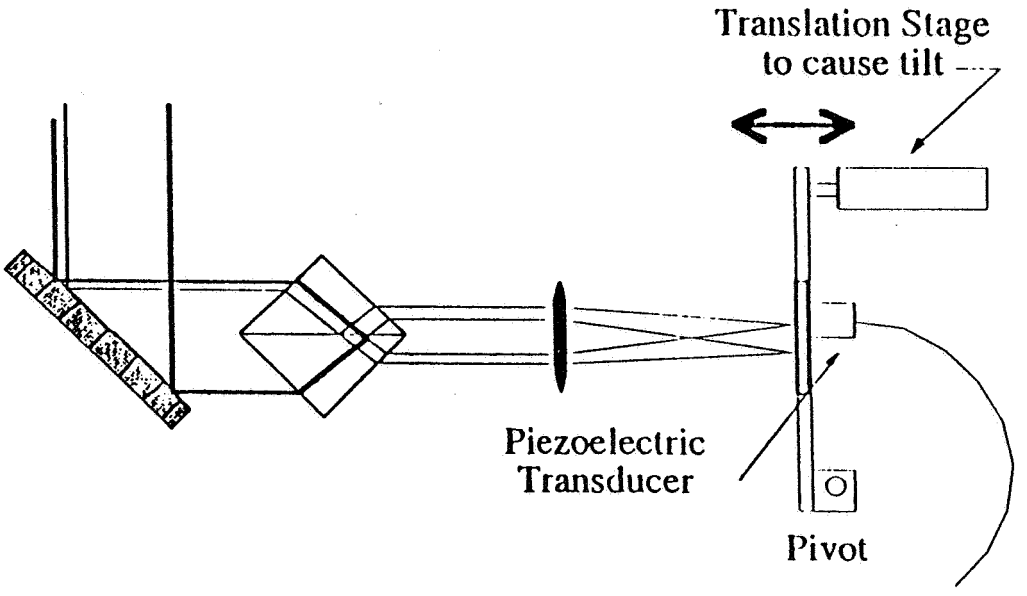

Figure 5: Interferometric detection of ultrasound generated with a piezoelectric transducer

The interferometer was converted to piezoreflective detection by blocking the reference beam. The piezoreflective signal from the aluminum coating remained linear as the voltage to the transducer was varied from 10 mV to 10 V (Figure 6).

The interferometer was converted back to interferometric detection, and the sensitivity of the interferometer was measured as a function of phase difference between the reference and signal arms. This relative phase change was accomplished for an interferometer in this configuration by tilting the specimen. The interference signal and the magnitude and phase of the interferometer signal are plotted in Figure 7. The interference curve exhibits the classic $1 + \cos\delta$ dependence. Since the excitation of the transducer and, therefore, the displacement of the surface of the specimen remains constants as the specimen is tilted, the interferometric signal will be proportional to the sensitivity of the transducer. This sensitivity is proportional to the slope of the interference curve which shows that the interferometer is operating as a classic Michelson interferometer. More importantly, this result demonstrates that the light in Ti:Sapphire laser pulses is coherent enough to use for interferometry.

4.2 Piezoreflective Detection of Laser-Generated Ultrasound

4.2.1 Arsenic Telluride

The piezoreflective detection of ultrasound was demonstrated to establish that the experiment was capable of reproducing the current state-of-the-art measurements. As_2Te_3 is a classic material to demonstrate piezoreflective detection because ultrasonic echoes produce large reflectivity changes in it. The specimen, from Humphrey Maris and Guray Tas at Brown University, had a 120 nm thick layer of As_2Te_3 on a silicon substrate. The experiment was configured in the piezoreflective mode (with the reference beam blocked). Data were acquired at a number of wavelengths to determine whether the piezoreflectivity of As_2Te_3 was wavelength dependent.

The ultrasonic echoes were clearly visible in all but the shortest wavelength data in Figure 8. Notice that the ultrasonic echoes are bipolar which is a result of the relatively low thermal conductivity of As_2Te_3. The curves in Figure 8 replicate the published data for As_2Te_3 [3].

4.2.2 Aluminum

Initial experiments to detect ultrasonic echoes in aluminum coatings on glass substrates failed. Upon further research it was discovered that the acoustic impedances of aluminum and glass were so similar that only 14% of the ultrasonic energy incident on the interface was reflected back. To increase the reflected ultrasound, a layer of gold was placed between the aluminum and glass which increased the amount of reflected ultrasound to 57%.

Scott Apt of the Materials Laboratory Characterization Facility produced specimens which had a 200 nm thick layer of aluminum evaporated on top a 300 nm thick layer of sputtered AuPd. The ultrasonic echoes from this specimen are clearly visible in Figure 9.

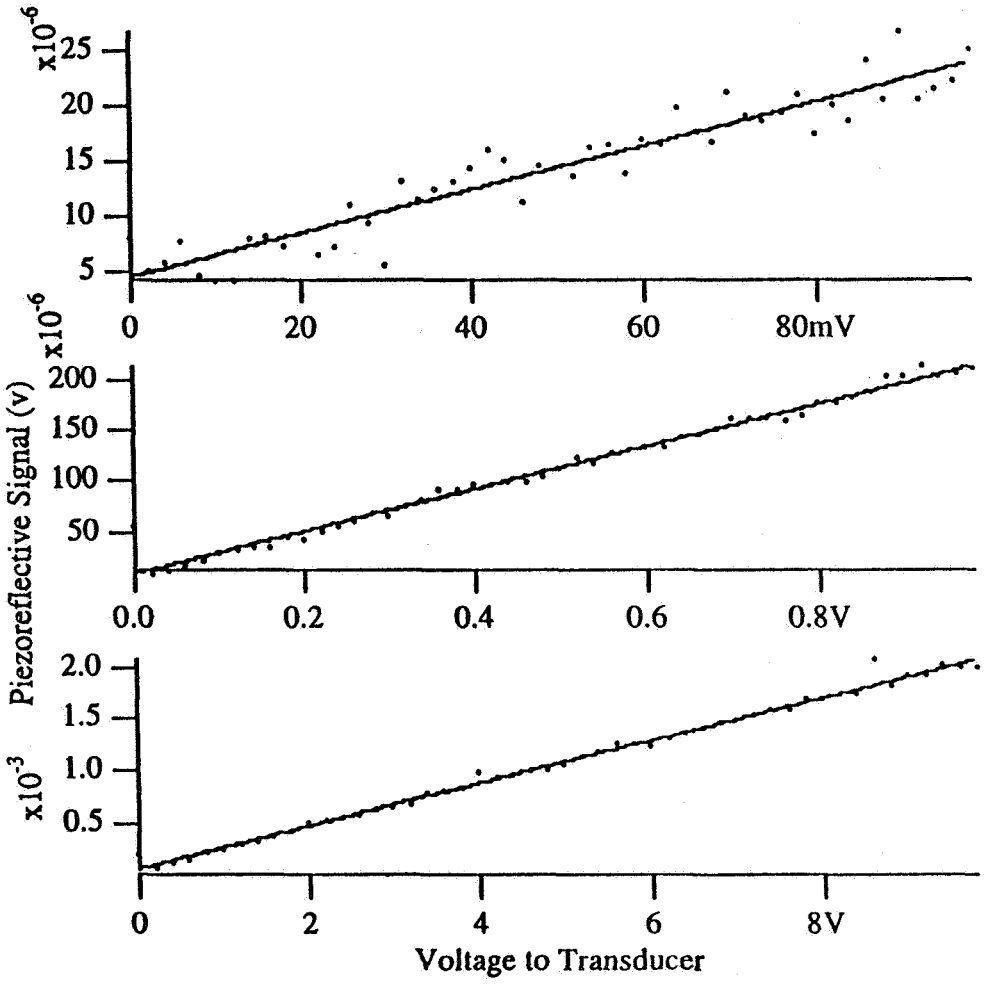

Figure 6: Piezoreflective signal as a function of voltage to the piezoelectric transducer

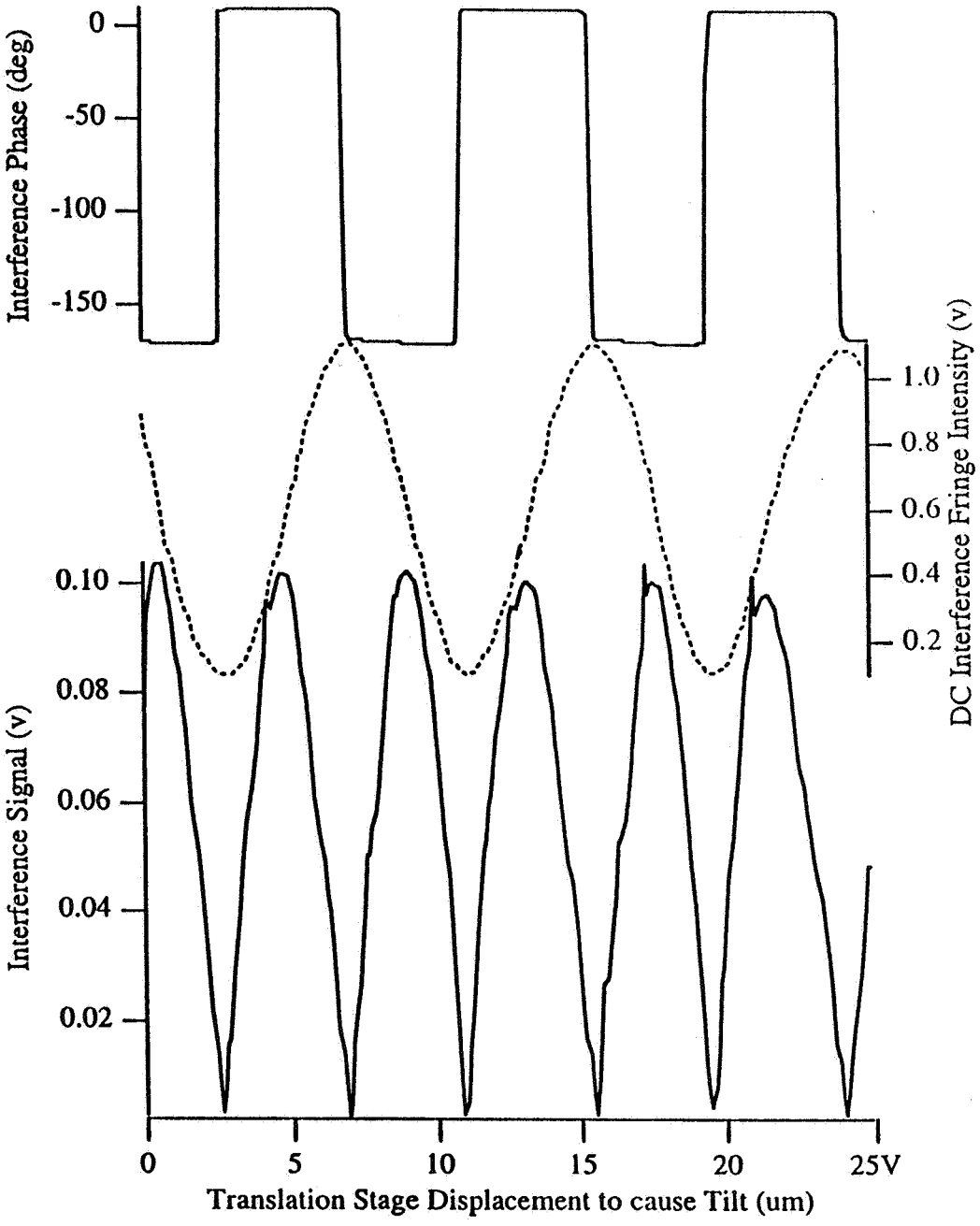

Figure 7: Interferometric signal as a function of phase delay between arms of the interferometer. The excitation was a 1 MHz piezoelectric transducer driven by 10v p-p sinusoid.

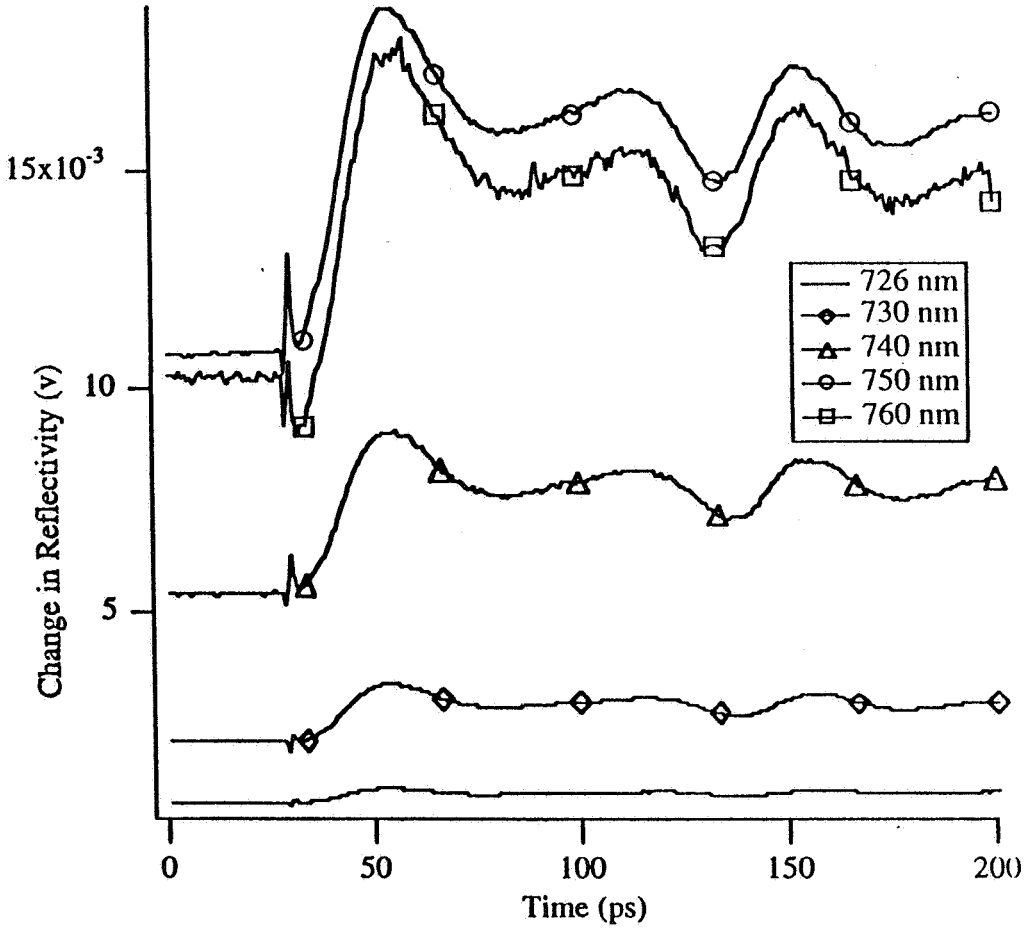

Figure 8: Piezoreflectivity of a 120 nm thick As_2Te_3 specimen

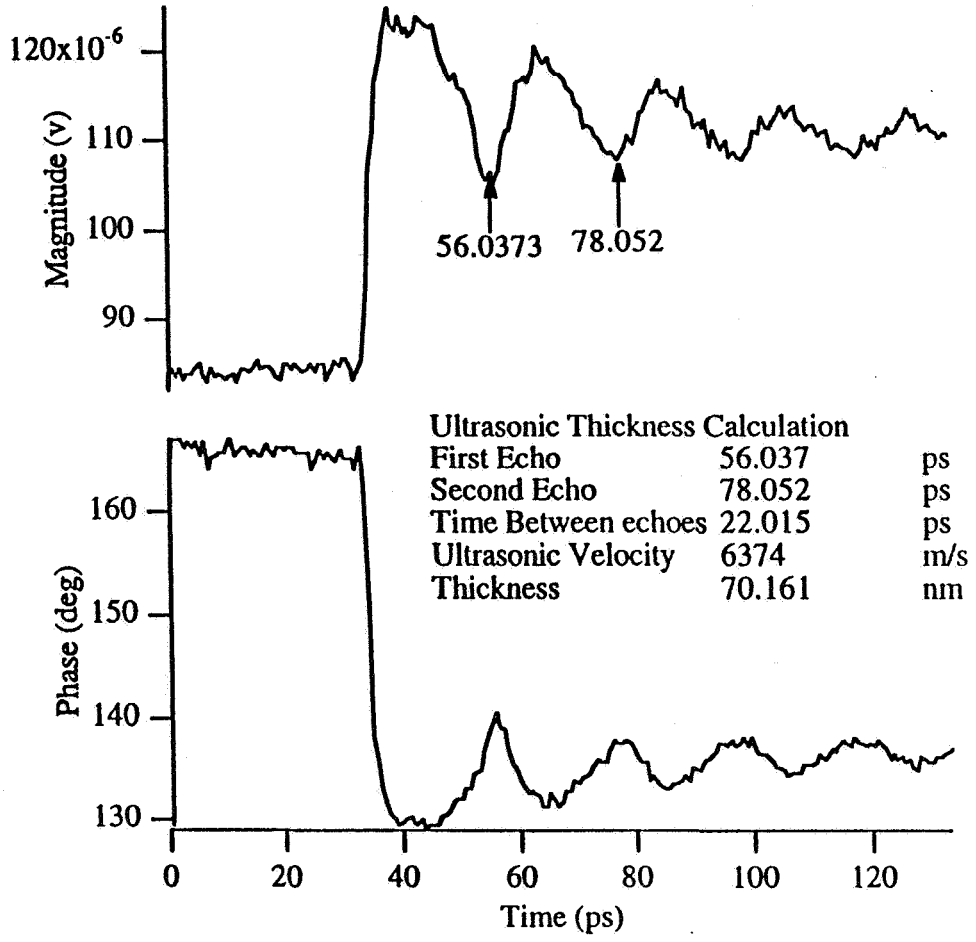

Figure 9: Piezoreflective detection of ultrasonic echoes in Aluminum

Figure 9 shows a thickness of 70 nm for the aluminum coating. This is significantly thinner than the 200 nm thickness of the coating. Until an independent measure of the film thickness is performed, it will be assumed that this error is due to a lack of process control on the evaporation process. Part of this discrepancy could be due to the fact that the properties of a thin coating (such as the ultrasonic velocity) are not the same as the properties for a bulk specimen of that materials, but normally this effect only changes properties by a few percent.

4.3 Interferometric Detection of Ultrasound

4.3.1 Aluminum

The 200 nm of Al over 300 nm of AuPd specimen was used to test the interferometer first because it had produced well defined piezoreflective ultrasonic echoes. The beam block was removed from the reference beam to convert the experiment to interferometric detection. The interferometric fringe pattern was then measured by scanning the tilt of the specimen. The thermal wave experiments verified that the sensitivity of the interferometer was indeed proportional to the slope of the interference curve and that the maximum sensitivity should occur at translation stage induced tilts of 16.0 μm, 23.9 μm, and 32.5 μm. Furthermore, the sensitivity at 16.0 μm and 32.5 μm should be the negative of the sensitivity at 23.9 μm which should show up in the phase data but not necessarily the magnitude data.

The data for a translation stage displacement of 23.9 μm, maximum positive sensitivity, was plotted first. The data, shown in Figure 10, has echoes in the same places as the piezoreflective data. Because the ultrasonic echoes are sharper in the interferometric data, it suggests that the interferometer may be better at picking up high frequencies than piezoreflective detection. The thickness of the aluminum layer was found from the ultrasonic echoes to be 67 nm.

To verify the interferometer performance, both sets of data from when the specimen was tilted to give the interferometer the maximum negative sensitivity were compared. The echoes should look the same but the phase should flip. Instead, the echoes vanished.

This interferometer behavior is definitely anomalous. When the interferometer is shifted from the maximum positive sensitivity to the maximum negative sensitivity, the ultrasonic echoes should still appear. Their disappearance suggests that the interferometric and piezoreflective effects have different phases and can add together constructively when in phase and can cancel each other when out of phase. To test this hypothesis, a specimen which was not piezoreflective and thermally reflective was required so that the only effect the interferometer saw would be the displacement of the surface.

4.3.2 Gold

Gold is an ideal material to test the interferometer because it has a piezoreflective signal which is 15 times smaller than the interferometric signal. A specimen with a 30 nm layer of gold over a 500 nm layer of SiO_2 on top of silicon was obtained from Humphrey Maris and Chris Morath at Brown University.

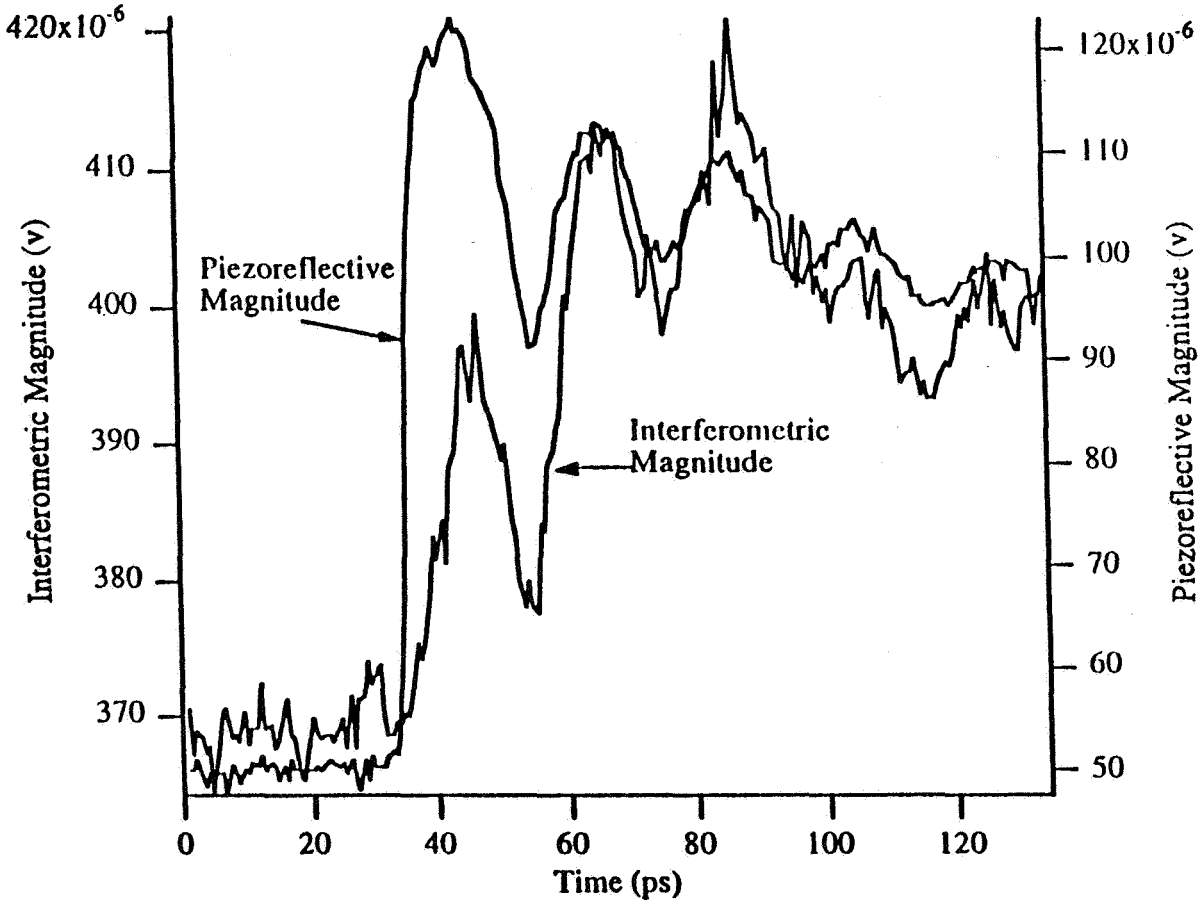

Figure 10: Interferometric vs. piezoreflective data, interferometer set for maximum positive signal

The difference between interferometric and piezoreflective detection is obvious in Figure 11. Both curves show a strong spike in the signal when the heating beam hits, but only the interferometric data shows ultrasonic echoes. If the scale of the piezoreflective data is enlarged, it is possible to see a single echo (Figure 12). Note that this is only a small echo with a signal-to-noise ratio close to 1, and if the specimen had been thicker, not even that echo would have been visible. These two plots shows that, for at least one material, interferometric detection is more sensitive than piezoreflective detection.

The interferometric data for several interferometer conditions are shown with the piezoreflective data for the gold specimen in Figure 13, and the ultrasonic echoes are clearly visible in the curve with the positive slope. It looks like there is an echo in the destructive interference curve, but it is not much larger than the noise. What is interesting is the way that the negative slope and destructive interference curves decrease in magnitude by approximately the same amount that the positive slope data increase in amplitude after the heating pulse hits. This is the behavior which was predicted for the interferometer. Unfortunately, the ultrasonic echoes, which should also be inverted, do not appear. This is probably due to a weak piezoreflective effect canceling a weak interferometric effect.

The quality of an interferometer is determined in part by its ability to detect a given displacement for a given frequency range. To determine the frequency response of the interferometer for this gold specimen, the Fourier transform of the ultrasonic echoes was taken. The displacement of the specimen was determined from the sensitivity of the interferometer. For this arrangement the sensitivity was found to be 0.00580 V/nm. The first ultrasonic echo showed a change in voltage of 40 μV, and the second showed a change of 23 μV. The displacement corresponding to a voltage change of 23 μV is 4.0 pm. This interferometer has a sensitivity of 4 pm for signals up to 100 GHz in frequency. For comparison, the properties of two reference beam interferometers may be compared to the delay line based pulsed interferometer[4].

4.3.3 Molybdenum

Molybdenum was demonstrated to have a low piezoreflectivity and was, therefore, useful to test the interferometer. The specimen consisted of a 200 nm thick layer of molybdenum over glass and was produced by Peter Shull at Johns Hopkins University. The magnitude data are shown in Figure 14 and the phase data in Figure 15.

These data are interesting because the size of the step caused by the heating of the surface of the specimen is proportional to thermal wave signal (the height of the curve before the heating beam hits). This suggests that the value of the thermal wave signal in Figure 14 is proportional to the sensitivity of the interferometer for a given tilt angle of the specimen and that this same sensitivity can then be used to calculate the height of the step caused by the absorption of the heating pulse.

A second feature to note is the flatness of the curves after the heating pulse is absorbed. Using a one-dimensional heat propagation model in an infinite half space, once a heating pulse is absorbed by the film the displacement of the surface of the film should remain constant due to

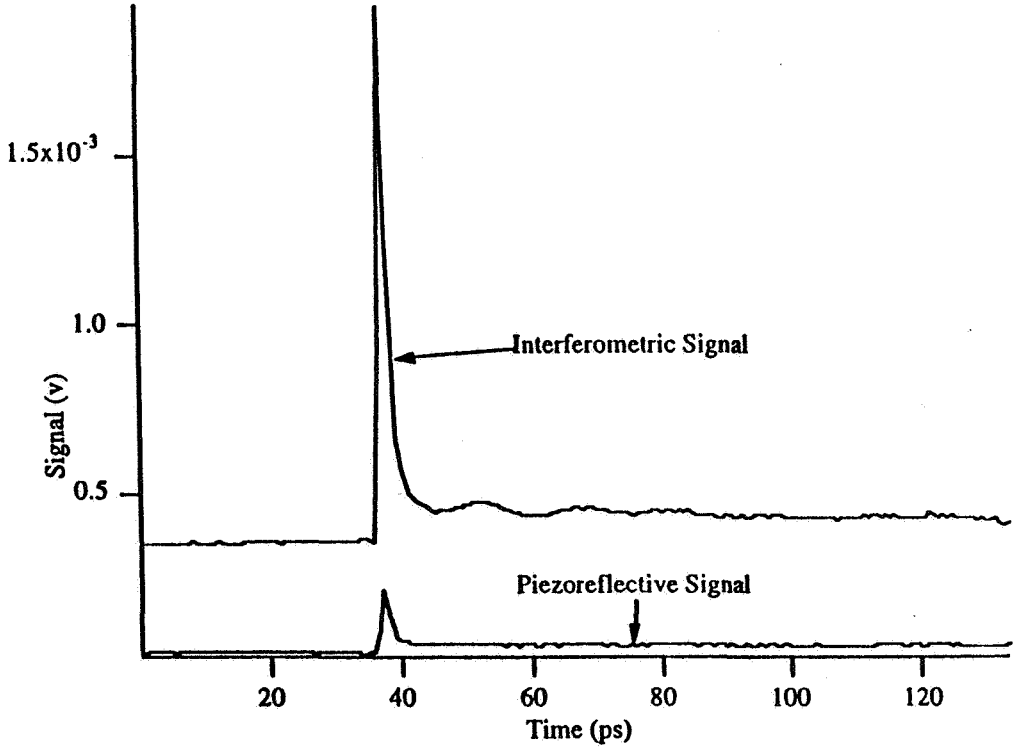

Figure 11: Interferometric and piezoreflective signal for a 30 nm gold coating

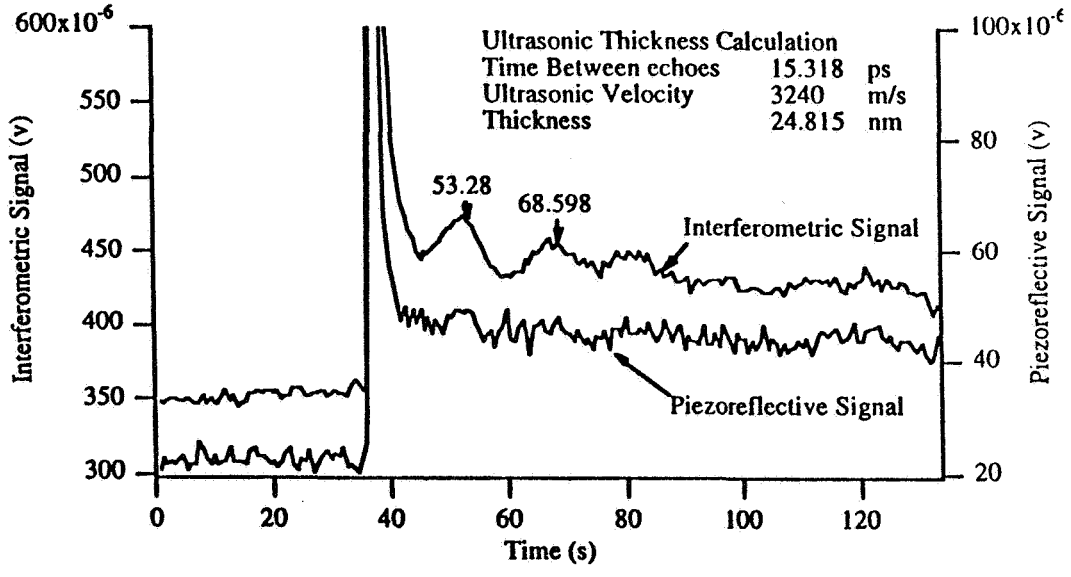

Figure 12: Interferometric vs. piezoreflective echoes - enlarged scale

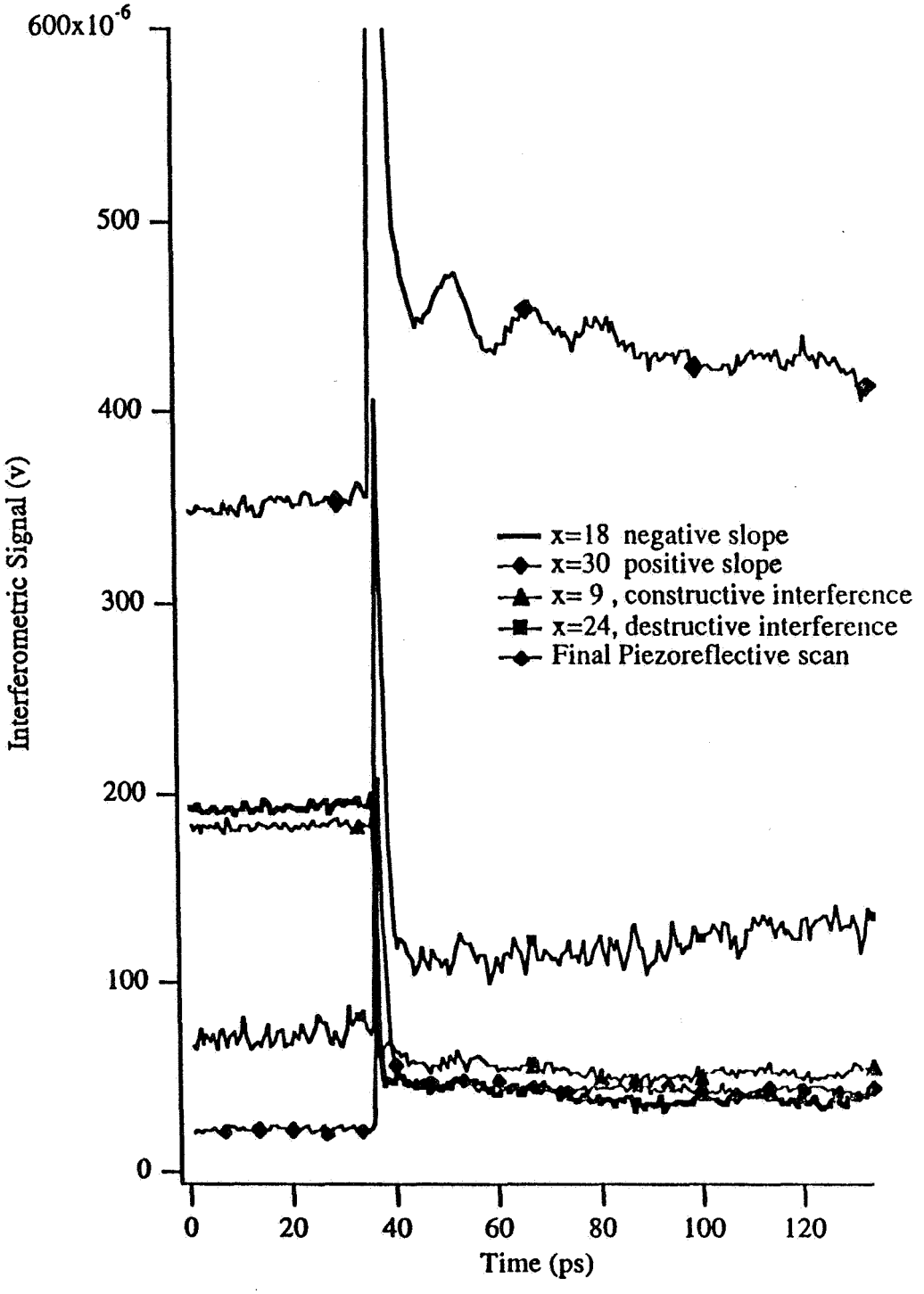

Figure 13: Magnitude data for the gold specimen

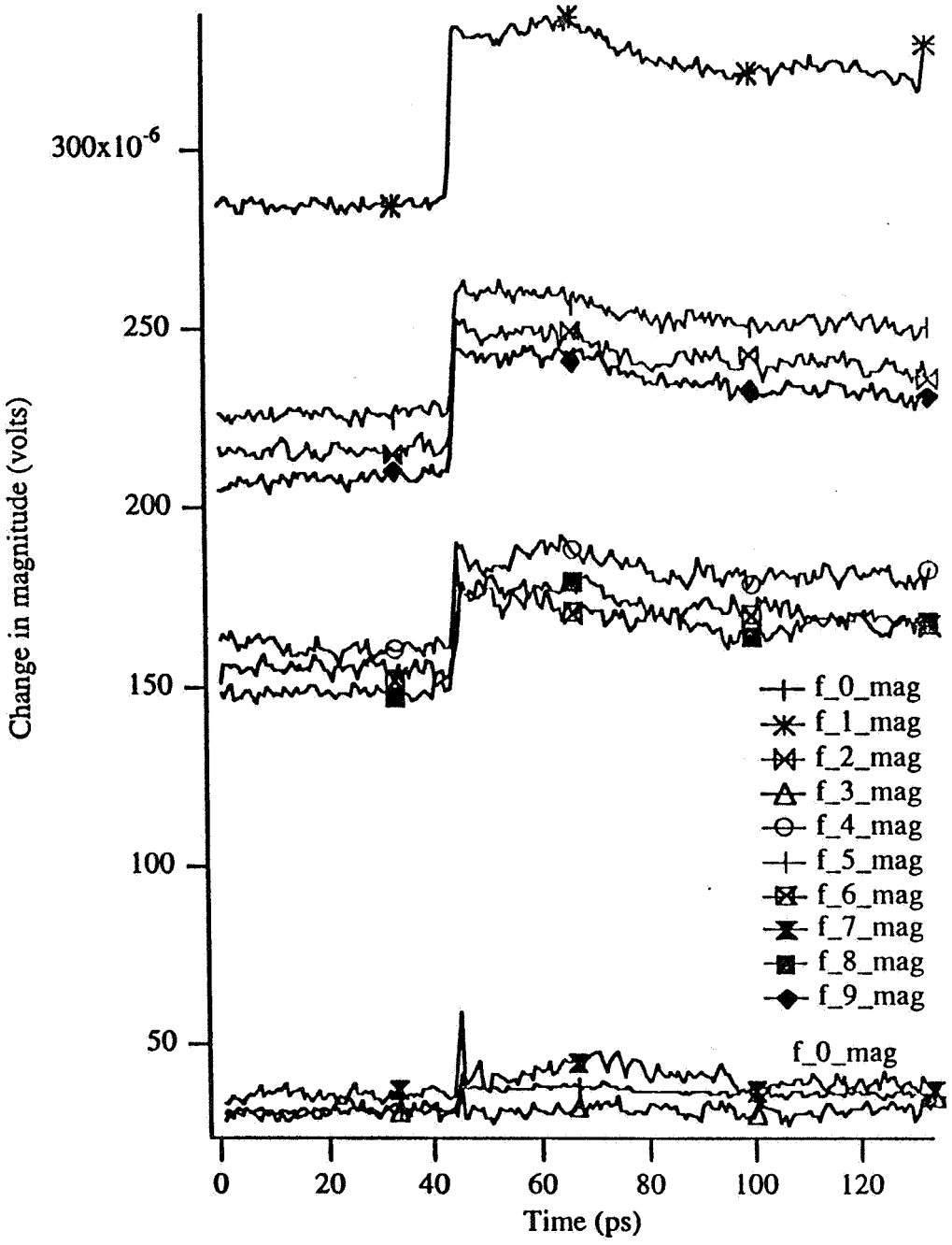

Figure 14: Magnitude data for molybdenum

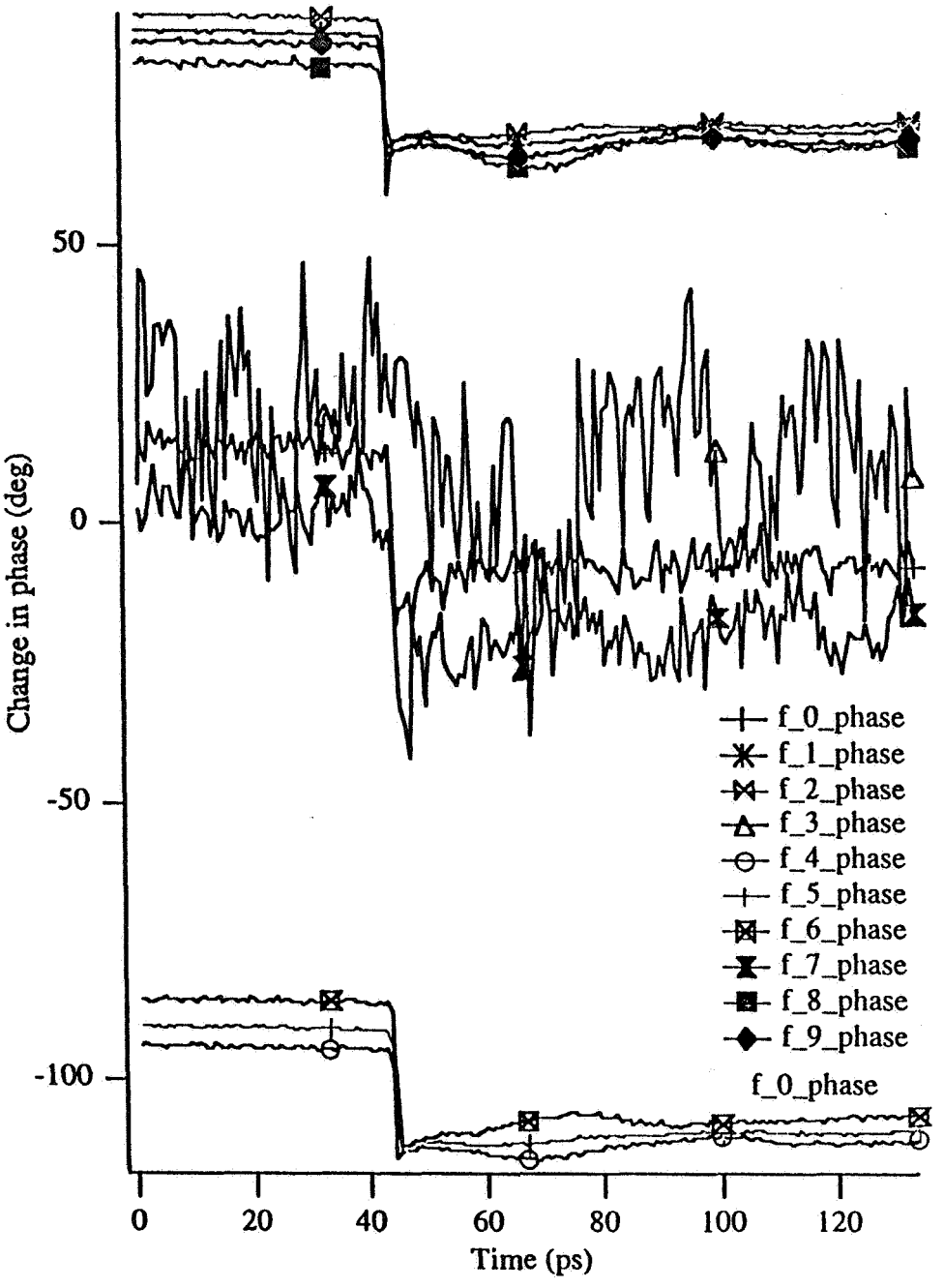

Figure 15: Phase data for molybdenum

conservation of energy. This would be seen experimentally as a step increase in the displacement of the surface of the specimen followed by no decrease in the signal. This is exactly what happens in Figure 14.

The thickness of the specimen, as measured from the interferometric data f1_mag, was 170 nm.

5. Conclusions

The objective of this effort was to develop a nondestructive inspection technique to measure the thickness of thin films. The inspection technique presented in this report, laser generated high frequency ultrasound with pulsed interferometric detection, has achieved this objective. Experimental results demonstrate that this technique measured the thickness of a 67 nm thick aluminum coating, a 25 nm thick gold coating, and a 170 nm thick molybdenum coating. Moreover, the data from the 30 nm thick gold coating show that the ultrasonic echo is only very weakly visible and would disappear into the noise if the coating were thicker. The interferometric data, however, clearly show three distinct echoes. In practice, to inspect gold coatings piezoreflectively, they would have to be coated with an aluminum transducer layer which would render the technique destructive. For materials which are not piezoreflective, interferometrically detected ultrasound is the better method for nondestructively measuring the thickness or elastic properties of the coating.

The delay line based pulsed interferometer has the same sensitivity as a conventional interferometer and a frequency range which is four orders of magnitude higher. Experiments using a piezoelectric transducer to generate ultrasound demonstrated that the light in ultrafast pulses from a Ti:Sapphire laser was coherent enough to perform interferometry. These results also show that the sensitivity of the interferometer to small displacements is proportional to the slope of the interference curve which demonstrates that the interferometer is operating in the same mode as a conventional Michelson interferometer. The frequency range of the interferometer was measured by transforming the ultrasonic echoes from a 30 nm thick gold coating into the frequency domain. Frequencies up to 100 GHz were observed for displacements as small as 4 pm. Conventional shot noise limited interferometers have a frequency range of only 10 MHZ for this sensitivity.

References

1. Scruby, C.B. and Drain, L.D. Laser Ultrasonics: Techniques and Applications. Bristol: Adam Hilger, 1990.

2. McKie, D.W. and Addison, R.C. "A Laser-based Ultrasound System Incorporating a Long Pulse Probe Laser for Increased Sensitivity." Review of Progress in Quantitative Nondestructive Evaluation, D.O. Chimenti and D.E. Thomson, eds., Plenum: New York, Vol. 13, 1994.

3. Thomsen, C., et al. "Surface Generation and Detection of Phonons by Picosecond Light Pulses," Physical Review B 34.6, 4129, 1986.

4. Scruby, C.B. and Drain, L.D. Laser Ultrasonics: Techniques and Applications. Bristol: Adam Hilger, 1990.